Francis Kotoka

Master of Science

Fouling Monitoring and Mitigation of Monovalent Selective Anion Exchange Membranes to Be Used in Reverse Electrodialysis

Dissertation for obtaining the Master of Science in Membrane Engineering

Erasmus Mundus Master in Membrane Engineering for a Sustainable World (EM3E-4SW)

Advisor: Dr. Svetlozar Velizarov (Nova University of Lisbon, Portugal)

Co-Advisor: Dr. Ivan Merino Garcia (Nova University of Lisbon, Portugal)

Jury:

President: Prof. Isabel Coelhoso (Nova University of Lisbon, Portugal)

Examiners: Prof. Andre Ayral (University of Montpellier, France)
Prof. Vlastimil Fila (University of Chemistry and Technology, Prague, Czech Republic),
Dr. Carla A.M. Portugal (Nova University of Lisbon, Portugal)
Dr. Svetlozar Velizarov (Nova University of Lisbon, Portugal)

Dissertation presented to Faculdade de Ciências e Tecnologia, Universidade Nova de Lisboa for obtaining the Master Degree in Membrane Engineering

28 July 2020

FACULDADE DE CIÊNCIAS E TECNOLOGIA
UNIVERSIDADE NOVA DE LISBOA

Fouling Monitoring and Mitigation of Monovalent Selective Anion Exchange Membranes to Be Used in Reverse Electrodialysis

The Erasmus Mundus Master in Membrane Engineering for a Sustainable Word (EM3E-4SW) is an education program financed by the European Commission - Education, Audiovisual and Culture Executive Agency (EACEA), under Project Number-574441-EPP-1-2016-1-FR-EPPKA1-JMD-MOB. It is also supported by the European Membrane Society (EMS), the European Membrane House (EMH), and a large international network of industrial companies, research centers and universities.

The European Commission's support for the production of this publication does not constitute an endorsement of the contents, which reflect the views only of the authors, and the Commission cannot be held responsible for any use which may be made of the information contained therein." (http://www.em3e.eu).

This Master thesis has led to the publication of two scientific articles namely:

- Kotoka, F., Merino-Garcia, I., and Velizarov, S., Surface Modifications of Anion Exchange Membranes for an Improved Reverse Electrodialysis Process Performance: A review Membranes 2020, 10(6), 134; https://doi.org/10.3390/membranes10080160
- Merino-Garcia, I., Kotoka, F., Portugal, C.A.M., Crespo, J.G., and Velizarov, S., Characterization of Poly(Acrylic) Acid-Modified Heterogenous Anion Exchange Membranes with Improved Monovalent Permselectivity for RED. Membranes 2020, 10(6), 134; https://doi.org/10.3390/membranes10060134

ACKNOWLEDGMENTS

I will like to acknowledge the European Commission-Education, Audiovisual and Culture Executive Agency (EACEA) who awarded my scholarship under the program of Erasmus Mundus Master in Membrane Engineering for a Sustainable World (EM3E-4SW), giving me the opportunity to participate through their esteemed Universities mobilities such as University of Montpellier (France), University of Toulouse III (Paul Sabatier, France), University of Chemistry and Technology (Czechia), and Nova University of Lisbon (Portugal).

Essentially, I am grateful to Dr. Svetlozar Velizarov and Dr. Ivan Merino Garcia for their great mentorship, training participation, insight and supervision during this study. Their enormous efforts have played very important role in my study and experience related to Anion Exchange Membranes for Reverse Electrodialysis, and electromembrane processes. Thus, I could not have enough words to express my appreciation.

My sincere gratitude goes to all the Professors who dedicated their time, energy, and knowledge during my academic training related to this program. Special thanks to Professor João Crespo, Professor Isabel Coelhoso, and Dr. Carla A.M. Portugal of Nova University of Lisbon for their academic lessons impacted on me in the field of membrane engineering.

I acknowledge the authorities of the Chemistry Department of Nova University of Lisbon (Caparica campus), for allowing me to undertake my experiments in the Laboratory.
My special appreciation to Dr. Samuel Kofi Tulashie, (of University of Cape Coast, Ghana) for accepting me as part of his family. His continuous mentorship, training, advice and support have developed me immensely.

Many thanks to my mother (Joyce Boakye), my brother Edward Baidoo, and wife Juliet Ackon for their supports throughout my academic, social, cultural, and physical wellness.
Finally, I acknowledge all my colleagues of EM3E-4SW who one way or the other have had significant impact on my development.

I give great Glory to Almighty God for a successful thesis.

ABSTRACT

Organic fouling phenomena predominantly restricts the behavior of Anion Exchange membranes (AEMs), thus reducing the obtainable net power density in reverse electrodialysis (RED). Consequently, we propose a monolayer surface modification of heterogeneous Ralex-AEMs with biocompatible poly(acrylic) acid (PAA) to enhance organic antifouling and monovalent membrane permselectivity. The AEMs were immersed in PAA aqueous solution for 24 h for surface modification. The modified membranes were physicochemical characterized via water contact angle (WCA), water uptake, ion exchange capacity, fixed charge density and swelling degree measurements. Their electrochemical characteristics were evaluated through cyclic voltammetry (CV), and electrochemical impedance spectroscopy (EIS). The impact of recurring fouling and cleaning was assessed. Membrane fouling behavior and sulfate rejection were studied in the presence of humic acid (HA), using model NaCl aqueous solutions in a diffusion cell. The modified AEMs (PAA-AEMs) showed a sulfate rejection improvement by 36%-54%, and their hydrophilicity was enhanced by > 15 % with respective to their WCA values. The 3 g/L PAA based AEM achieved an antifouling resistance of 65.8% towards HA in comparison with the unmodified membrane. Recurring fouling and cleaning of the membranes was investigated using 25 ppm HA as the model foulant, and 0.1 M $NaOH_{(aq)}$ as the cleaning agent. In this case, the NaOH cleaning solution restored the membrane resistances almost to their original values after the first fouling and cleaning cycle. However, it failed in the second and third cycles due to the predominance of irreversible fouling and adsorption caused by the HA, leading to higher membrane resistance. Overall, the results demonstrate the technical feasibility of the proposed membrane surface modification procedure, and the need for efficient cleaning agents to mitigate fouling of AEMs. This study may therefore provide a viable approach to enhance RED process efficiency.

Keywords: Reverse Electrodialysis; Membrane Fouling Mitigation; Anion Exchange Membranes; Monovalent Permselectivity; Polyacrylic acid Modification

Table of Contents

INDEX OF FIGURES

INDEX OF TABLES

ABBREVIATIONS

ABBREVIATION	NAME
AEM	Anion Exchange Membranes
AFM	Atomic Force Microscopy
AMS	2-acryloylamido-2-methylpropanesulfonic acid
ATR-FTIR	Attenuated Total Reflectance Fourier Transform Infrared Spectroscopy
Both sides 3 g/L PAA	Two Sides Membrane Modification with 3 g/L PAA
BSA	Bovine Serum Albumin
CD_{fix}	Fixed Charge Density
CEM	Cation Exchange Membranes
CLSM	Confocal Laser Scanning Microcopy
CPE	Constant Phase Element
CV	Cyclic Voltammetry
DBL	Diffusion Boundary Layer
DC	Direct Current
ΔRm	Change in Membrane Resistance
ED	Electrodialysis
EDL	Electrical Double Layer
EIS	Electrochemical Impedance Spectroscopy
GO	Graphene Oxide
GO-AEM	Graphene Oxide Modified AEM
HA	Humic Acid
HACC	Hydroxypropyl trimethyl ammonium chloride chitosan
HCC	High Concentration Solution
IEC	Ion Exchange Capacity
IEM	Ion Exchange Membrane
I-V	Current-Voltage
LbL	Layer-by-Layer
LCC	Low Concentration Solution
LSV	Linear Sweep Voltammetry
MBA	N,N-methylenebis(acrylamide)

ABBREVIATION	NAME
m_{dry}	Mass of Dry Membrane
MF	Microfiltration
m_{wet}	Mass of Wet Membrane
NOM	Natural Organic Matter
NSBC	N-O-sulfonic acid benzyl chitosan
NZVI	Nanoscale zero-valent iron
OCV	Open Circuit Voltage
OM	Optical Microscopy
One side 1 g/L PAA	One Side Membrane Modification with 1/g/L PAA
One side 3 g/L PAA	One Side Membrane Modification with 3/g/L PAA
One side 5g/L PAA	One Side Membrane Modification with 5/g/L PAA
PAA	Polyacrylic acid
PAA-AEM	Polyacrylic acid modified AEM
PAAS	Poly(sodium acrylate)
PAH	Poly(allynamine hydrochloride)
PDA	Polydopamine
PEI	Poly(ethyleneimine)
PI	Photo Imaging
PSS	Poly(sodium 4-styrene sulfonate)
PVA	Polyvinyl Alcohol
RED	Reverse Electrodialysis
SBOS	Sodium Octylbenzene-sulfonate
SBS	Sodium Benzene-sulfonate
SD	Swelling Degree
SDBS	Sodium Dodecylbenzenesulfonate
SDS	Sodium Dodecylsulfonate
SEM	Scanning Electron Microscopy
SGP	Salinity Gradient Power
SOS	Sodium Octylsulfonate
SPPO	Sulfonated poly(2,6-di-methyl-1,4-phenylene oxide)

ABBREVIATION	NAME
UF	Ultrafiltration
UV-VIS	Ultraviolet-Visible Spectrophotometry
WCA	Water Contact Angle
WU	Water Uptake

SYMBOLS

SYMBOL	NAME	UNIT
α	Measured Membrane Permselectivity	
$\propto_{AEM}$	Theoretical Permselectivity of Anion Exchange Membrane	
$\propto_{CEM}$	Theoretical Permselectivity of Cation Exchange Membrane	
$\propto_{SO4^{2-}}^{Cl^-}$	Chloride/Sulfate Permselectivity	
α_{HCC}	Activity of High Concentrated Salt Solution	
α_{LCC}	Activity of High Concentrated Salt Solution	
C	Capacitance	F
C_{DBL}	Diffusion Boundary Layer Capacitance	F
C_{EDL}	Electrical Double Layer Capacitance	F
$[Cl^-]$	Chloride Concentration in the Receiver	mmol/L
δ	Membrane Thickness	cm
Δ_{exp}	Measured Membrane Potential	Volt
Δ_{th}	Theoretical Membrane Potential	Volt
F	Faraday Constant	C/mol
f	Frequency	Hz
I_{DC}	Applied Direct Current	A
I_{Ld}	Current of External Load	A
I_o	Output Alternating Sinusoidal Current	A
I_t	Input Alternating Sinusoidal Current	A
j_{Cl^-}	Chloride Flux	mmol/(hm^2)

SYMBOL	NAME	UNIT
j_{dl-}	Diffusion Flux	mmol/(hm^2)
j_i	Total Ionic Flux	mmol/(hm^2)
j_{mi}	Migration	mmol/(hm^2)
j_{vi}	Convection flux	mmol/(hm^2)
k	Imaginary number related to EDL	
l	Imaginary Number Related to DBL	
n	CPE Exponent	
OCV_{th}	Theoretical Open Potential	Volt
ϕ	Phase Shift	
P_W	Power Density of Membrane Stack	W/m^2
Q	Constant Phase Element Parameter	Fcm^{-2}S$^{(n-1)}$
R	Universal Gas Constant	J/(mol K)
R_{DBL}	Diffusion Boundary Layer Resistance	Ω
R_{EBL}	Electrical Double Layer Resistance	Ω
R_{is}	Internal Stack Resistance	Ω
R_{LD}	Resistance of External Load	Ω
R_m	Electrical Resistance of Membrane	Ω
R_{m+s}	Ohmic Resistance of Membrane and Solution	Ω
$R_{non-ohm}$	Non Ohmic Resistance	Ω
R_{ohm}	Ohmic Resistance	Ω
R_s	Electrical Resistance of Salt Solution	Ω
S	Area of Membrane	cm^2
σ	Specific Conductivity	S/cm
$[SO_4^{2-}]$	Sulfate Concentration in the Receiver	mmol/L

SYMBOL	NAME	UNIT
T	Absolute Thermodynamic Temperature	K
t	Time	s
U_b	Total Voltage Measured Across Blank Salt Solution	Volt
U_T	Total Voltage Measured Across Membrane	Volt
V_t	Input Alternating Sinusoidal Voltage	Volt
V_o	Output Alternating Sinusoidal Voltage	Volt
ω	Circular frequency	rad/s
Z	Impedance	Ω
|Z|	Impedance Modulus	Ω
Z'	Real Impedance	Ω
Z''	Imaginary Impedance	Ω
z_{an}	Valency of Anion	
z_{cat}	Valency of Cation	
Z''_{CPE}	Imaginary Impedance of CPE	Ω
z_i	Valency of the Ion	
Z_T	Total Impedance	Ω

1 INTRODUCTION

The study of membrane-based processes has extensively attracted the attention of the research community and industries since 1940 [1], owing to the possibility of separating liquid-liquid, solid-liquid mixtures and gas-gas mixtures. In spite of the several challenges, the establishment of reverse osmosis, electrodialysis, microfiltration and ultrafiltration processes and their commercial applications in the mid-1960s and late 1970s intensified the development of membrane science and technology [2, 3].

The continuous consumption of fossil fuels for energy production has resulted in climate change concerns [4]. In this context, the atmospheric concentration of carbon dioxide (CO_2) has increased by more than 30% since pre-industrial times [4], reaching 417.07 ppm in May 2020 [5]. Nowadays, the use of membranes for power generation is emerging due to the need for alternative renewable and sustainable ways, triggered by the increasing trend of global energy demands, which is expected to reach an annual consumption of 778 Etta Joule by 2035, reaching 80% in 2050 [4, 6, 7]. In May 2020, the renewable energy generation increased to almost 28% of the global energy share [8]. As a result, several environmentally friendly energy sources are extensively explored such as solar energy, biofuels, wind energy, fuel cell technology and salinity gradient power (SGP) process [9, 10]. The key elements of most of these interesting technologies are the membranes.

In this respect, SGP represents one of the new areas of expertise that incorporates membranes for sustainable power generation [11, 12], being the second largest marine-based energy source with high potential global power production (2.4-2.6 TW), which may significantly contribute to the global electricity demand [13]. Thus, the available vast ocean and rivers in the world could be used to generate clean energy via electro-membrane processes. Although different processes have been already proposed for SGP such as electrodialysis (ED), one of the most interesting approaches is the Reverse Electrodialysis (RED) technology, where the heart of the process is the application of alternatively stacked cation exchange membranes (CEMs), and anion exchange membranes (AEMs) [11, 12, 14]. The so-mentioned ion exchange membranes (IEMs) allow the exchange of ions (according to their charge and the nature of the membrane) between the high salt concentration stream (*i.e.,* seawater) and the diluted one (*i.e.* river or brackish water), hence generating ionic current [15]. This ionic current is then converted to electric current using redox reactions at the electrodes which are placed at the end of the stack of membranes. However, several aspects usually limit the application of commercial CEMs and AEMs, such as reduced permselectivity(α), high electrical resistances, and fouling phenomena, loss of operation stability, among others [16-18], which lead to a reduced power output from RED.

Fouling is one of the main phenomena that hinders the performance of IEMs in RED systems. The membranes used are prone to biofouling, organic fouling, colloidal fouling, and scaling, thus reducing the monovalent permselectivity and the electrical conductivity of the IEMs [19-21]. Therefore, they decrease the membrane efficiency, stability and durability. Besides, negatively charged foulants (*e.g.,* HA that can be found in river water, and divalent ions such as sulfate (SO_4^{2-}) interact with the fixed charged group of the AEMs, which involves a reduction of the open circuit voltage (OCV), and the corresponding, obtainable power density from RED [22-24]. Consequently, the control of the

monovalent permselectivity and fouling phenomena in AEMs is essential for achieving an improved RED process efficiency. Accordingly, various studies in literature focus on enhancing the mentioned properties of AEMs, considering materials selection, addition of chemicals, and surface modifications procedures [25-27].

Several methods and approaches are available to carry out surface membrane modifications [28] such as adsorption, polymerization, ion implantation, solution casting, electric deposition, and plasma treatment, among others, in order to either modify the surface chemical structure or add new layer/s on membrane surface [29-32]. Surface modification has proven to be excellent for enhancing the antifouling properties and monovalent permselectivity. The purpose of the additional layer(s) incorporated onto the surface of AEMs is therefore to improve membrane hydrophilicity-hydrophobicity ratio and the surface charge density, to modify roughness, to increase the rejection of multivalent ions, to induce antimicrobial properties, and to enhance membrane homogeneity, among others [30-33]. It is also worth noting that the physicochemical, electrochemical, and mechanical characteristics of the selected pristine membranes and the modifying agents utilized should be compatible with the purpose of achieving the above-mentioned desirable membrane properties after surface modification.

In this regard, polyacrylic acid (PAA) can improve the membrane hydrophilicity and surface charge density, while reducing the impact of multivalent ions at the same time. Thus, its use has been considered in literature to modify several CEMs in an attempt to achieve excellent results, including enhanced hydrophilicity and improved antifouling properties [34-37]. Besides, through Donnan effect which is very effective for monovalent-divalent anions separation[38], the PAA negative layer could strongly reject large number of divalent anions before they enter the AEM, and enhances the migration of monovalent anions. Despite this fact, to the best of our knowledge, PAA has not been proposed to modify AEMs, even though it was used as foulant for AEMs in 1998 [39]. Therefore, the aim of this study is to modify the surface of commercial heterogeneous AEMs with PAA in order to render a monovalent permselectivity while mitigating fouling phenomena at the same time. HA and model streams containing NaCl (aqueous solutions) were used as foulant and streams with different salinity, respectively. A comprehensive membrane characterization (physicochemical and electrochemical), including mass transport experiments (for 24 h) was assessed.

Since this study is focused on membrane surface modification, the membranes were also deliberately fouled to evaluate the ability of NaOH to restore the membranes via cleaning. The membrane electro-resistance was measured after fouling and cleaning in each case.

1.1 BACKGROUND AND MOTIVATION

1.1.1 MOTIVATION

The estimated global energy output from estuary is 30 TW from which 2.6 TW could be recovered [12, 40, 41]. Therefore, utilizing RED to harvest such massive energy can significantly contribute to the green and sustainable energy share, and reduction in global warming related to excessive CO_2 emission [42]. The first RED pilot plant generated a very promising power output of 65W and stabilized within 5 months of operation, in 2016 [43]. The prototype scale-up was projected to produce a power output in the order of 1 kW, indicating the advance progress in RED for energy generation.

Since organic foulants and SO_4^{2-} in natural water bodies hinder the operational stability, power efficiency, and thus retarding the commercial operation of RED, we know that it is important to mitigate them simultaneously to improve the RED process. Nevertheless, preparing novel AEMs to simultaneously overcome fouling and achieving higher monovalent permselective membranes obviously involve higher costs, and takes longer time to be developed compared to the improvement of existing AEMs, which have the potential to achieve desirable characteristics via surface modification.

Moreover, as environmentally friendly and effective methods are preferable, it is required to develop eco-friendly modifying agents to render the mentioned properties in AEMs for RED applications. With respect to this, PAA represents a relatively green, non-toxic, and readily available substance which could be used [34-37]. This study may therefore provide novel insights to the knowledge of improving RED process performance and its efficiency through AEM surface modification with eco-friendly PAA.

1.1.2 THEORETICAL BACKGROUND OF RED

The heart of RED systems relates to alternatively CEMs and AEMs arranged in series of stacks, as shown in **Figure 1**. These IEMs are responsible for the effectiveness and efficiency of RED, using natural feedwaters of different salinity gradient. However, the presence of foulants and multivalent ions (*e.g.,* Mg^{2+}, $Ca^{2+}$and SO_4^{2-}) cause an uphill transport which reduces the OCV and thus, the obtainable power density [22, 44]. The salinity gradient between the high concentrated salt solution, HCC (*e.g.,* seawater), and low concentrated solution, LCC (*e.g.,* river water) causes ionic energy generation which is then converted to electrical energy through redox reaction at the anode and cathode.

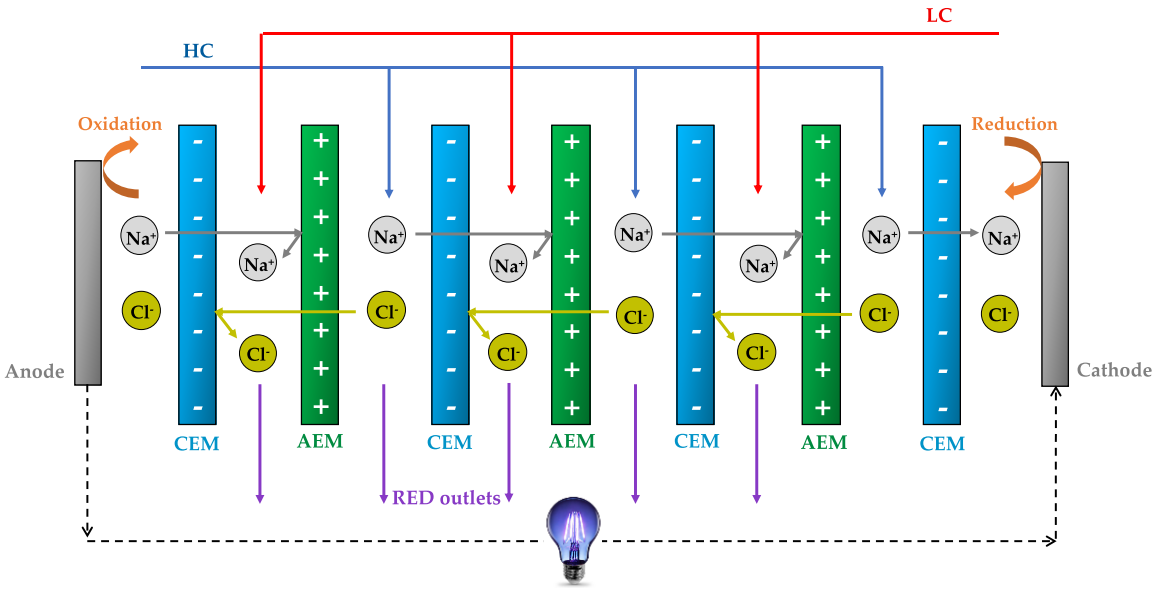

Figure 1 *RED compartment showing stacks of IEMs*

The transport phenomenon occurring in IEMs for RED systems is expressed by the Nernst-Planck equation (**Eqn. 1**), which includes the total ionic flux (j_i), due to migration (j_{mi}), diffusion flux (j_{di}) and convection flux (j_{vi}). The total flux depends on the diffusivity of the ionic species (D_i), concentration of the ionic species (c_i), mobility of ions (u_i), electric potential (φ), and fluid velocity (v).

$$j_i = j_{di} + j_{mi} + j_{vi} \tag{1}$$

Where $j_{di} = -D_i \nabla c_i; j_{mi} = -u_i c_i \nabla \varphi; j_{vi} = v c_i$

The major parameters that influence the performance of the process are the ion exchange capacity (IEC), fixed charge density (CD_{fix}), permselectivity (α) and electrical resistance. IEC represents the number of fixed charges within the IEM per unit dry mass of the membrane, whereas CD_{fix} relates to the number of fixed charges attached to the polymer backbone [15]. The CD_{fix} highly depends on the water uptake (WU) and the IEC of the membrane under investigation. These figures of merit determine the transport of counter ions, permselectivity and electrical resistance of the membrane [44]. The permselectivity demonstrates the membrane capability to exclude co-ions while allowing the passing of counter ions. This process is strongly driven by Donnan exclusion [45]. The mentioned crucial parameters are expressed in the following equations (from **Eqn. 2** to **Eqn. 6**):

The permselectivity is expressed by the relation between the experimentally measured membrane potential ΔE_{exp}, and theoretical membrane potential (ΔE_{th}):

$$\propto = \frac{\Delta E_{exp}}{\Delta E_{th}} \times 100 \tag{2}$$

Considering a total (100 %) monovalent selective membrane, the theoretical membrane potential is determined by the ratio of the activity coefficient between the HCC and LCC, according to the Nernst equation.

$$\Delta E_{th} = \frac{RT}{F} ln \left(\frac{a_{HCC}}{a_{LCC}}\right)^{\frac{1}{z_i}} \quad (3)$$

Nevertheless, the total potential with no current load for a stack of membranes (see **Figure 1**) is the OCV of the membrane cell. Hence, considering N as the number of membrane pairs, the theoretical OCV can be expressed as follows:

$$OCV_{th} = \frac{NRT}{F}\left(\propto_{CEM} ln\left(\frac{a_{HCC}}{a_{LCC}}\right)^{\frac{1}{z_{cat}}} + \propto_{AEM} ln\left(\frac{a_{HCC}}{a_{LCC}}\right)^{\frac{1}{z_{an}}}\right) \quad (4)$$

Where R, T, F and z are the universal gas constant, absolute thermodynamic temperature, Faraday's constant and valency of ion respectively. The OCV is higher when z is 1, indicating the importance of monovalent ion selectivity to RED power output.

Furthermore, the electrical resistance of the membrane is also an essential parameter which significantly influences the performance of AEMs for RED applications. The internal stack resistance (R_{is}), as indicated in **Eqn. 5**, comprises both the ohmic (R_{ohm}) and non ohmic ($R_{non\text{-}ohm}$) resistances. The R_{ohm} is the sum of the membrane(s) resistance (R_m) and the salt solution resistance (R_s), whereas the $R_{non\text{-}ohm}$ refers to the resistance associated with charge transfer limitations which is the sum of the electrical double layer (EDL) and diffusion boundary layer (DBL) resistances [44, 46].

$$R_{is} = R_{ohm} + R_{non-ohm} = (R_m + R_s) + (R_{EDL} + R_{DBL}) \quad (5)$$

Theoretically, **Eqn. 6** shows that the power density (P_W) generated by the stack of membranes connected to an external load exponentially depends on the OCV, the internal stack resistance, R_{is} and external load, I_{Ld} .

$$P_w = {I_{Ld}}^2 R_{Ld} = \left(\frac{OCV_{th}}{R_{is}+R_{Ld}}\right)^2 \times R_{Ld} \quad (6)$$

Considering **Eqn. 4**, **5** and **6**, the resistance of the membranes must dramatically be reduced and controlled to increase the performance of the process, especially, when several membranes are used in series. In addition, the monovalent permselectivity should also be increased. Therefore, the approach considered in the present work intends to modify AEMs to enhance not only the monovalent membrane permselectivity, but also the antifouling behavior, which is crucial for the practical implementation of this technology.

1.1.3 BACKGROUND ABOUT FOULING IN ION EXCHANGE MEMBRANES

Despite the interesting potential of the RED technology for blue energy harvesting, fouling phenomena ,especially in AEMs, represents a major limitation that must be overcome. In this case, AEMs are extremely affected by negatively charged foulant, mainly present in river water streams, which can be classified into organic fouling and colloidal fouling [19-21].

Colloidal foulants have excessive negative surface charges. For instance, they could exist as aluminum silicate clay minerals, colloidal silica, organic colloids, and oxides of iron, manganese and aluminum in natural streams [47, 48]. Due to these excessive negative charges, such foulants interact undesirably with the positively fixed charged groups of the AEMs via electrostatic forces. Thus, the concentration of dissolved salts, pH, temperature, fouling particle concentration, operational mode and hydrodynamic conditions, among others, are the main factors which influence colloidal fouling [33]. Therefore, it is required to introduce antifouling surface characteristics to reduce the adverse interactions between the AEMs and the colloids.

Different organic foulants such as proteins, oils, carbohydrates, antifoaming agents, and aromatic compounds (*e.g.,* HA) also affect the behavior of AEMs [49-51]. They are dissolved in the RED feed streams, and covalent bonds dominate in them [52]. These foulants are mostly negatively charged and adhere to the positive charged groups of the AEM due to their large molecular size. Their adhesion to the membrane is attributed to hydrophobic and electrostatic interactions. Similar to colloidal foulants, different membrane properties, the operational mode, the concentration, size and structure of the organic foulant greatly influence the associated fouling behavior [33]. Besides, the high solubility of organic foulants in RED feed streams make them abundant in different natural streams that can be used for RED applications. In fact, the adverse effects of organic and colloidal fouling on the electrochemical properties of AEMs for RED systems is considerable, and requires significant attention because they highly increase the membrane electrical resistance and compromise the monovalent permselectivity of the membrane under consideration [17, 49, 51]. To understand the behavior of the foulants, various characterization methods must be employed. This determines which modification method is suitable to control and mitigate fouling. Overall, the modification of the membrane surface under study is indispensable to induce higher hydrophilic properties, which may reduce the adhesion of the organic foulants onto the surface of AEMs.

1.1.4 THEORITICAL PRINCIPLE OF ELECTROCHEMICAL IMPEDANCE SPECTROSCOPY (EIS)

1.1.4.1 REPRESENTATION OF EIS IN NYQUIST AND BODE'S PLOT

Direct current measurement (DC) allows the quantification of the total resistance (R_{DC}) as shown in **Eqn. 7**, which corresponds to the sum of R_m, R_{EDL} and R_{DBL} in EIS [53]. Thus, DC does not discriminate

the R_m, R_{EDL} and R_{DBL}, however, in RED systems, the resistances due to charge transfer limitations such as the electrical double layer and the diffusion boundary layer effects (represented in **Figure 2**) must also be investigated. Thus, a more powerful tool than DC measurements is needed to measure the mentioned resistances.

$$R_{DC} = \frac{U_T - U_b}{I_{DC}} \tag{7}$$

Where U_T represent total voltage measured across the membrane and the solution; U_b is the voltage measured from the blank solution; I_{DC} is the applied direct current.

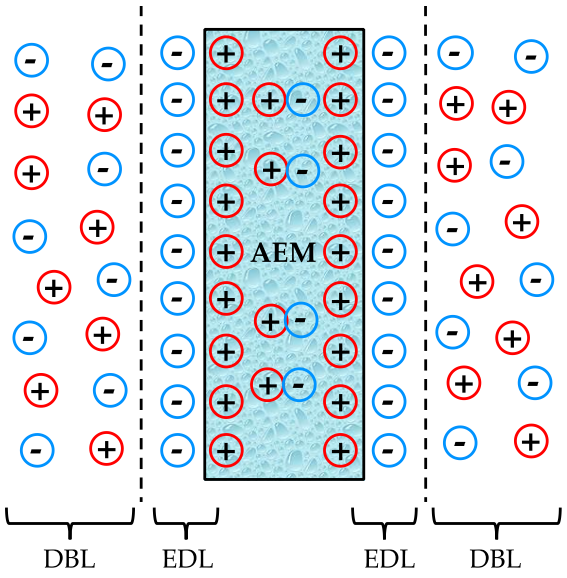

Figure 2 *Representation of an AEM with EDL and DBL effects*

EIS is a complex electrochemical characterization non-destructive technique which reveals the electrochemical characteristics of multilayer systems, electrochemical reactions, transport properties of materials, dielectric properties, complex surfaces, electrical resistances (R_m, R_{EDL} and R_{DBL}), and electrical conductance of membrane materials [54]. In this method, an alternating sinusoidal current or voltage is applied to electrodes pairs at fixed frequency range. The response shows the phase shift (ϕ) and the impedance (Z) as a function of the frequency (f) range selected. The input alternating sinusoidal voltage (V_t) and the output alternating sinusoidal voltage (V_o) relating to the frequency and time (t) are expressed in **Eqn. 8**. Similarly, the input alternating sinusoidal current (I_t) relates to the output alternating sinusoidal current (I_o) according to **Eqn. 9**.

$$V_t = V_o \sin(2\pi f t) = V_o\, e^{(k\,2\pi f t)} \tag{8}$$

$$I_t = I_o \sin(2\pi f t + \phi) = I_o\, e^{k(2\pi f t + \phi)} \tag{9}$$

Where k is an imaginary number.

The frequency is related to the angular velocity (ω) as:

$$\omega = 2\pi f \tag{10}$$

From Euler's formula:

$$e^{k\phi} = cos\phi + k\, sin\phi \tag{11}$$

At zero ϕ ,the time variation of the voltage, the current, and impedance are related according to Ohms law as:

$$Z = \frac{V_t}{I_t} \tag{12}$$

Considering the impedance and the frequency, the combination of **Eqn. 8**, **9** and **12** results in:

$$Z = \frac{V_t}{I_t} = \frac{Vo\ \ e^{(k\,2\pi ft)}}{Io\ \ e^{k(2\pi ft+\phi)}} = |Z|e^{-k\phi} = |Z|cos\phi - k|Z|sin\phi \tag{13}$$

Where |Z| is the impedance modulus.

The impedance has real (Z') and imaginary (Z'') parts, usually demonstrated in Nyquist's and Bode's plots. These parameters are expressed as follows:

$$Z' = |Z|cos\phi \tag{14}$$

$$Z'' = |Z|sin\phi \tag{15}$$

The real and imaginary parts of the impedance are demonstrated in the polar coordinate, as represented in **Figure 3**.

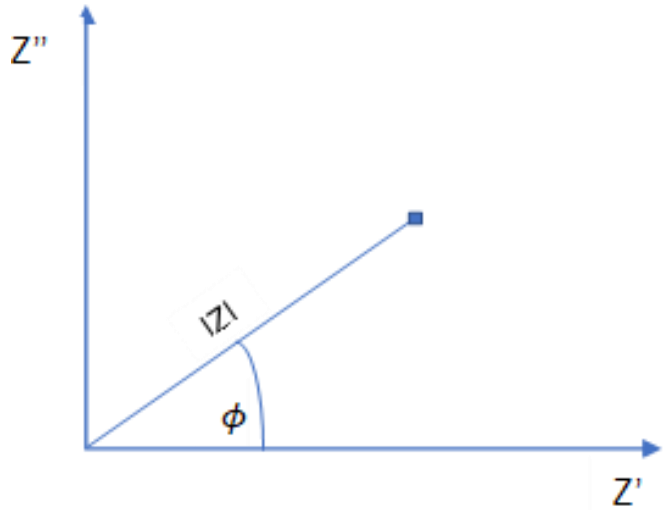

Figure 3 *Polar coordinate showing the rea and imaginary part of the impedance*

1.1.4.2 EIS REPRESENTED IN AN EQUIVALENT CIRCUIT MODEL

The EIS method also provides information about the thickness of membrane interface and effective capacitance, which relates to membrane surface microstructure, ion transport, and electrical properties [55]. To determine the membrane electro-resistance and other necessary parameters from EIS, we consider different approaches in this work, including the combinations of resistances, capacitance, and

constant phase element (CPE) in series or parallel. These parameters are described by the equivalent circuit model as represented in **Figure 4**. The equivalent circuit depicts the ohmic resistor (from the membrane and solution resistance (R_{m+s}) connected to charge transfer resistors in series (R_{EDL} and R_{DBL}) or parallel combinations with either capacitance (C) or CPE [42].

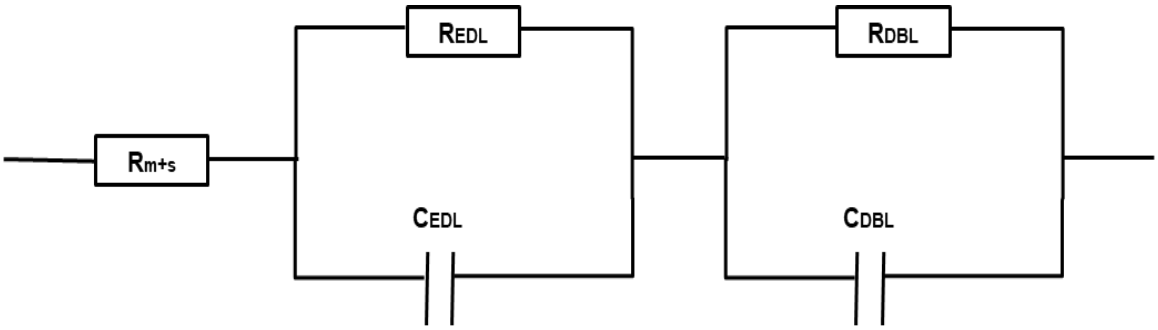

Figure 4 *Equivalent circuit diagram showing electrical double layer, and diffusion boundary layer resistance*

Ideally, for a homogeneous interface such as smooth and ordered surfaces, the capacitance relates to the imaginary impedance as expressed in **Eqn. 16** [42]:

$$-Z'' = \frac{1}{2\pi fC} = \frac{1}{k\omega C} \tag{16}$$

However, in most real and practical applications, the capacitance is substituted by CPE, due to interphase heterogeneity such as surface roughness and disorder [53, 56-58]. In this case, in a real heterogenous system interface, the evolution of the EDL, and DBL resistances can be obtained at medium and lower frequencies, respectively. The CPE parameter (Q) relates to the CPE imaginary impedance (Z'') as expressed in the following equations [42]:

$$-\mathrm{Z''_{CPE}} = \frac{1}{(\mathrm{k}\,2\pi\mathrm{f})^{\mathrm{n}}\mathrm{Q}} = \frac{1}{(\mathrm{k}\omega)^{\mathrm{n}}\mathrm{Q}} \tag{17}$$

Where *n* is the empirical parameter exponent of CPE ($0 \leq n \leq 1$).

If n is equal to 1, **Eqn. 17** transforms into **Eqn. 16** (Q=C), representing an ideal homogeneous and orderly membrane surface.

The total impedance of the system (Z_T) is the sum of the real and imaginary impedance. Considering ohmic resistor in series to a parallel combination of the electrical double layer and diffusion resistors, with their capacitor, the Z_T is expressed in **Eqn. 18** [58, 59]

$$Z_T = Z' - jZ'' = R_{m+s} + \left(\frac{R_{EDL}}{1+(\omega R_{EDL}C_{EDL})^2} - k\frac{\omega R_{EDL}{C_{EDL}}^2}{1+(\omega R_{EDL}C_{EDL})^2}\right) + \left(\frac{R_{DBL}}{1+(\omega R_{DBL}C_{DBL})^2} - l\frac{\omega R_{DBL}{C_{DBL}}^2}{1+(\omega R_{DBL}C_{DBL})^2}\right) \tag{18}$$

At lower frequencies, the electrical conductivity of the interface becomes lower than membrane resistance, demonstrating that the interface act as a membrane insulator, resulting in a higher overall resistance, as shown in **Eqn.19**. In this regard, $1 \gg (\omega R_{EDL}C_{DL})^2$ (considering that $\omega = 2\pi f$), the EDL layer significantly impacts the total impedance of the system [58, 59].

$$Z_T \cong R_{m+s} + R_{EDL} - k\omega R_{EDL}{C_{DL}}^2 + R_{DBL} - l\omega R_{DBL}{C_{DBL}}^2 \cong R_{m+s} + R_{EDL} + R_{DBL} \tag{19}$$

Where *I* is an imaginary number

However, between high and medium frequencies, the diffusion term is negligible. Since the dielectric permittivity of the diffusion interface becomes higher than the membrane, current passes easily through the membrane with negligible resistance. When diffusion is neglected, **Eqn. 19** transforms to **Eqn. 20**.

$$Z_T \cong R_{m+s} + R_{EDL} + R_{DBL} \cong R_{m+s} + R_{EDL} \quad (20)$$

At higher frequencies, $(\omega R_{EDL} C_{DL})^2 \gg 1$, implying that the membrane resistance dominates the restriction of current flow [58, 59], and reduces **Eqn. 18** to **Eqn. 21**.

$$Z_T \cong R_{m+s} \quad (21)$$

Considering **Eqn. 18**, **19**, **20** and **21**, the R_{m+s}, R_{EDL}, and R_{DBL} can easily obtained from the EIS data, which is fitted to the optimum equivalent circuit model, considering the χ^2 error function provided by the software of the potentiated used.

1.2 OBJECTIVES

Considering the increased demand of clean, renewable and sustainable energy, numerous technologies have recently emerged to tap energy from various natural sources such as water bodies, sunlight, wind and biomass [9, 10]. The recovery of SGP from the sea, brackish water and river water via RED is one of the dominant clean energy sources which has caught researchers attention [11, 12, 14]. However, the presence of multivalent ions as well as fouling phenomena limit the desirable behavior, especially, monovalent permselectivity, of AEMs which forms part of the “heart” of RED systems, thus reducing the obtainable net power density and stability. Organic foulants in the LCC feed stream predominantly restrict RED systems. To overcome these issues, surface modification of AEMs to induce excellent antifouling properties and high multivalent rejections is an essential approach.

Therefore, the aim of this master thesis is to propose a negative charge monolayer modification procedure to functionalize commercial heterogeneous AEMs using PAA as the modifying agent to improve the monovalent permselectivity and the antifouling behavior of the membrane by enhancing its hydrophilicity [34-37]. It may increase the negative charge density of the AEM by forming a negative surface layer to improve divalent anion rejection.

Thus, the objectives of the present thesis are as follows:

- To modify Ralex AM-PES Commercial AEMs with PAA.
- To investigate the effects of PAA concentration during modification.
- To carry out the physicochemical and electrochemical characterization of the modified membranes.

- To conduct time dependent mass transport experiments on the modified membranes, thus determining their Cl^-/SO_4^{2-} permselectivity.
- To monitor organic antifouling properties of the modified AEMs using HA as the model foulant.

2. LITERATURE REVIEW

2.1 FOULING MONITORING, CONTROL, CHARACTERIZATION, AND MITIGATION METHODS

Ion exchange membrane fouling can be monitored, controlled and/or characterized by several methods, depending on the application. In RED, some of the IEMs fouling monitoring, control and characterization techniques applied are usually similar to conventional membrane applications such as Microfiltration (MF), Ultrafiltration (UF), Nanofiltrations (NF), and Reverse Osmosis (RO) (**Figure 5**) [60, 61]. These methods are mainly based on visualization, membrane characteristics, qualification and quantification [33].

2.1.1 FOULING CHARACTERIZATION BY VISUALIZATION

Visualization methods identifies the color, structure, and distribution of the foulants either inside or at the surface of the IEMs. These methods mainly include Confocal Laser Scanning Microcopy (CLSM, **Figure 5 a**), Atomic Force Microscopy (AFM, **Figure 5 b**), Scanning Electron Microscopy (SEM), Optical Microscopy (OM), and Photo Imaging (PI) techniques [33]. PI was used to visualize the fouling (**Figure 5 c**) of an AEM, with further studies revealing that the foulant was a 97%-based protein [62]. The photograph showed that the foulants occurred at the interface between the AEM and the casein solution.

In other studies, SEM images were used to observe biofouling on a Cellulose acetate/Chitosan-based membrane. The image revealed that bacteria (*Escherichia coli*) is adhered to the surface of the membrane (**Figure 5 d**) after 4 h of contact with solution containing the bacteria [63]. The biofouling was attributed to its higher hydrophobicity compared to other membranes investigated. SEM also identified the formation of a gel-layer (**Figure 5 e)** on a Fujifilm Type 10 AEM when the membrane was exposed to produced water [64]. That resulted in a rapid buildup of the membrane potential.

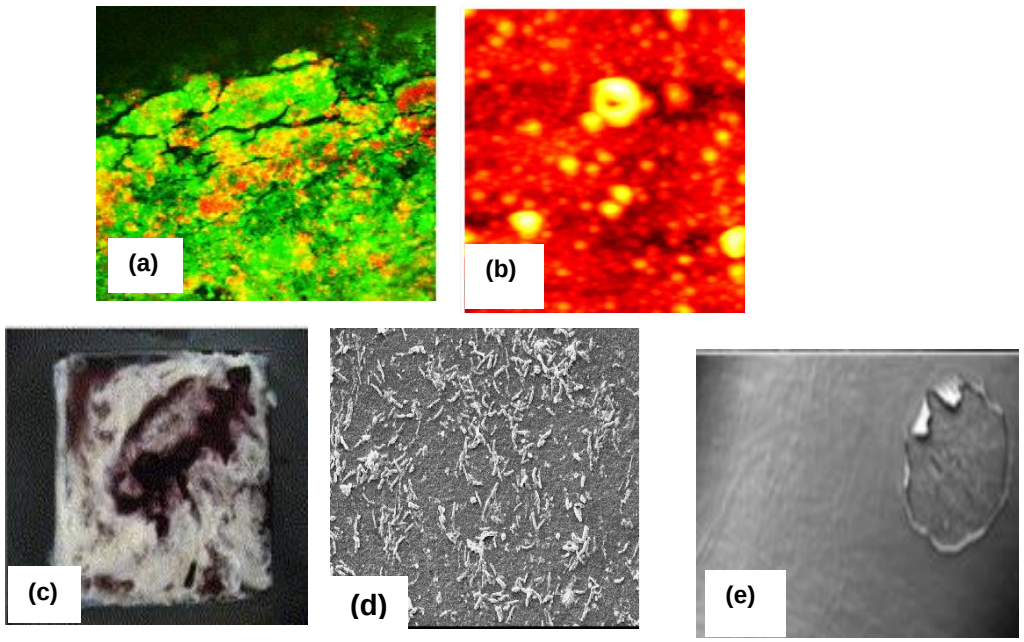

Figure 5 *Images showing foulants visualized by CLSM (a), AFM (b), PI(c) and SEM (d and e) [60-64].*

2.1.2 FOULING MONITORING, CONTROL AND CHARACTERIZATION BASED ON MEMBRANE PROPERTIES

Monitoring foulants based on the membrane characteristics identifies the changes in the electrochemical, mechanical, dimensional and swelling properties of the IEMs caused by the foulants. In this case, the common properties of the IEM characterized are the membrane electrical resistance, conductance, and hydrophilicity or hydrophobicity ratio [42]. Belaid et. al , and Lteif et. al. proposed that the electrical resistance of the membrane can be determined by measuring the specific conductivity (σ) of the membrane by using a pair of platinum electrodes contained in a clip cell [65, 66]. Thus, the specific conductivity of the membrane is inversely related to its electrical resistance (**Eqn. 25**). After observing the electrical resistance and conductivity of the pristine membrane, the occurrence of membrane fouling increases the electrical resistance due to decreasing electrical conductivity.

The contact angle allows to determine the hydrophilicity and hydrophobicity at the membrane surface caused by the foulants [67]. Usually, a more hydrophobic membrane translates to high membrane resistance and vice versa. Therefore, IEMs are generally prepared to have higher hydrophilicity-hydrophobicity ratio. This improves the wetting of the membrane, rendering a higher antifouling potential, leading to a lower electro-resistance [67, 68].

Interestingly, monitoring, controlling and characterization methods are not only limited to the resistance, conductivity, and contact angle. Other studies apply more exhaustive approaches such as voltammetry, electrochemical impedance spectroscopy, chronopotentiometry, transport number, zeta potential, and spectrophotometry to determine the physicochemical and electrochemical properties of the membrane [42, 69-72].

$$R_m = \frac{\delta}{\sigma S} \quad (22)$$

Where δ is the thickness of the membrane, and S is the active electrode area.

2.1.2.1 FOULING MONITORING AND CHARACTERIZATION VIA EIS AND DC MEASURMENTS

EIS provides details of the increase in the total resistance caused by fouling phenomena. In this case, the foulants adversely escalates the membrane thickness, which increases the overall resistance related to R_m, R_{EDL} and R_{DBL} due to lower electrical conductivity, and poor charge transfer induced by the foulants [42, 67, 69]. For instance, a study investigated the fouling effects of 1 wt.% Bovine Serum Albumin (BSA) on a Neosepta AMX at current densities levels ranged from 0 A/m^2 to 14 A/m^2. The authors showed that at 6.5 A/m^2, the resistance of the BSA foulant alone exceeded the sum of the R_{m+s}, R_{EDL} and R_{DBL} by 23.5% [69]. In another literature, the monitoring and characterization of fouling in RED systems using Fujifilm CEM and AEM Type 1 (FUJIFILM Manufacturing Europe BV, the Netherlands) revealed that sodium dodecylbenzenesulfonate (SDBS) used as the model foulant increased stack ohmic resistance by 83.5% [70]. Since the fouling experiment was conducted for more than one day (60 h), and the degree of fouling depended on the concentration of the foulant, they attributed the extreme escalation in the ohmic resistance to the absorption and surface adsorption of the SDBS onto the IEMs, which reduced the active membrane area. The EIS results are often compared with current-voltage (I-V) to establish the reliability of the data. Comparing the total resistance from the EIS with the I-V curve of voltammetry provides essential similarities and high accuracy between the electrochemical measurements.

In DC measurements, information on the I-V curve can be obtained, hence, the ohmic polarization, limiting current density, and overall resistance, according to ohm's law is determined [53, 70, 73, 74]. The overall resistance obtained from the I-V curves is equivalent to the sum of the Rm, R_{EDL} and R_{DBL} from EIS. For instance, previous work carried out on homemade AEMs characterization demonstrated that the total resistance measured from I-V compared with EIS differed by only 2% maximum [53]. Similarly, a comparable trend was recorded in Fujifilm CEM and AEM Type 1 for the DC and EIS in the presence of SDBS in river water [70].

2.1.2.2 FOULING MONITORING AND CHARACTERIZATION USING CHRONOPOTENTIOMETRY

Chronopotentiometry is a very important electrochemical measurement for determining the antifouling potential of a membrane [72, 75]. In this case, fixing the current density and measuring the time evolution of the potential shows the transition time where there is a higher jump in the measured potential. The resistance registered by the foulant extremely increases the membrane potential at constant current. In other words, a higher potential jump indicates that the membrane has been fouled,

while a shorter transition time indicates that the membrane is susceptible to fouling [76-78]. This concept is clearly investigated in literature, where the antifouling potential of a commercial Homogeneous ASE (Astom Crop, Japan), Neosepta AMX (Astom Corp., Japan), Heterogeneous AEM (Zhe-jiang Qian-qiu Environmental Protection & Water Treatment Co. Ltd., China), and Neosepta ASM (Astom Crop, Japan), was evaluated [72, 75-78]. They used SDBS model foulant, which is predominantly known for causing severe organic fouling, even though other foulants such as sodium octylsulfonate (SOS) and sodium dodecylsulfonate (SDS), sodium benzene-sulfonate (SBS), and sodium octylbenzene-sulfonate(SBOS) were also studied. For instance, the antifouling potential measured in a commercial Homogeneous ASE (Astom Crop, Japan) showed that the foulants fouls the unmodified membranes rapidly under 240 mins with rapid increment in the measured potential, reaching 1.2 V. However, the dopamine modified membrane exhibited higher antifouling potential in long term operation (more than 1300min) with a potential below 0.3 V [76]. The longer transition time exhibited by the modified ASE indicates a higher antifouling potential compared to the pristine membrane. The researchers attributed the enhanced antifouling potential of the modified membrane to the improved surface hydrophilicity, which reduced the adhesive interaction between the SDBS and the membrane.

2.1.2.3 FOULING CHARACTERIZATION FROM TRANSPORT NUMBER

Another important fouling characterization based on membrane properties is the transport number or flux of ions [67]. The ratio of the flux (j_i) between two competing ions in solution is the permselectivity. Transport number provides indications of the presence of fouling because fouling often influences the counter ion migrations through the ion exchange membranes [17, 79]. In RED, and ED, the competing anions mostly considered for permselectivity (see **Eqn. 23**) are Cl^- and SO_4^{2-} in the low concentrated feed compartment [67, 68, 78]. The permselectivity provides indications on the performance of the membrane since it translates into the OCV and power density as represented in **Eqn. 4** and **6**. This means the presence of sulfate ions in the RED streams obviously reduce the power density. In this context, Pintossi et al. studied the impact of SO_4^{2-} on power density considering Fujifilm Type I, Fujifilm Type 10, Neosepta AMX-fg, and Neosepta ACS standard grade monovalent selective membranes. They demonstrated that the presence of sulfate ions in RED system increases the electrical resistance, leading to losses in the normalized power output up to 25% [24]. Similarly, the study of utilizing homemade and Neosepta ACS AEMs showed that the presence of sulfate drops the gross power density by 17.8% at a flow velocity of 0.76 cm/s [68], unaffecting the ACS membrane significantly. However, the introduction of 10 mg/L HA as the model foulant decreased the power density of both the homemade and ACS membranes appreciably. The authors attributed this effect to the uphill transport of sulfate and membrane fouling, which increased the electrical resistance of the membranes.

$$\propto_{SO4^{2-}}^{Cl^-} = \frac{j_{Cl^-}/[Cl^-]}{j_{SO4^{2-}}/[SO4^{2-}]} \tag{23}$$

Where $[Cl^-]$ and $[SO4^{2-}]$ are the respective concentrations of chloride and sulfate ions in the receiver compartment (where no sulfate was initially present). j_{Cl^-}, and $j_{SO4^{2-}}$ are the flux of chloride and sulfate ions in the receiver compartments, respectively

2.1.2.4 FOULING CONTROL BASED ON ZETA POTENTIAL

Zeta potential is another interesting fouling characterization technique that could be applied depending on the properties of the membrane. The zeta potential relies on many conditions including the surface roughness, charge, chemical heterogeneity, pH, temperature, composition and concentration of the solutions [80, 81]. It reveals the degree of electrostatic attraction or repulsion between the membrane and the foulant [82, 83], enabling researchers to control the associated electrostatic interactions between the membrane surface and the foulants. In this regard, Kim et. al investigated the impact of natural organic matter (NOM) on the zeta potential at different pH [84]. They achieved a good relationship between the quantity of adsorbed NOM and the zeta potential. In another study, the effects of humate on Neosepta AMX, ACM, AM-1 and AMV showed that it has more negative values of -18 mV to -25 mV over the whole pH range [85]. The humate fouled the AMX and shifted the isoelectric point to a higher pH, with the zeta potential starting from a more positive value than the pristine. The given information is essential for predicting and controlling organic fouling phenomena on different IEMs. Actually, Park et al. proposed a way to deal with humate fouling in ED, using a Neosepta AMX [86]. The humate recorded higher negative zeta potential of -30 mV. To mitigate its fouling, the authors added various separate water-soluble polymers, namely, poly(ethyleneimine) (PEI), poly(acrylic acid (PAA), and poly(vinyl alcohol) (PVA) to the feed solution. The PEI exhibited the highest positive zeta potential (+14 mV) and interacted highly with the humate, thereby, reducing the humate charge and forming interpolymer complex which hindered the fouling of the anion exchange membranes. Therefore, the feed did not need filtration. Besides, the formed interpolymer complex did not decline the ED performance. Contrarily, as a result of electrostatic repulsion, the PAA and PVA rarely forms interpolymer complex with the humate.

2.1.3 QUALITATIVE AND QUANTITATIVE FOULING CHARACTERIZATION

The qualitative and quantitative procedures are based on evaluating the chemical composition of the foulants, functional groups, and the amount of such foulants present at the surface or inside the membrane [33].

Qualitatively, Attenuated Total Reflectance Fourier Transform Infrared Spectroscopy (ATR-FTIR), and UV-Visible Spectrophotometry (UV-VIS) are mostly applied to characterize the foulants on the membranes related to the chemical composition, though UV-VIS can also be used for quantification. The ATR-FTIR unveil the functional groups in the foulants. For example, AT-FTIR detected protein and peptides fouling of Neosepta AMX-SB in the wavenumber regions of 1600 cm^{-1} and 1580 cm^{-1}-1510 $cm^{-1,}$ representing amide I and amide II, respectively [87]. Other authors used ATR-FTIR to determine the appearance of amide I and amide II at 1662 cm^{-1} and 1322 cm^{-1} when polyacrylamide fouled an AEM [88]. Two peaks at 3349 cm^{-1} and 3196 cm^{-1} representing -NH_2 of primary amides were also detected.

Quantitatively, the UV-VIS determines the amount of the compound of interest at a specific wavelength [17]. Thus, it is widely used to determine the presence of organic fouling phenomena. For instance, the quantity of BSA, SDBS, and humate were measured via UV-VIS after being used as model foulants for AEMs [69, 83, 86].

Other techniques such as Chromatography, Mass Spectrometry (MS), Emission Spectrometry, Energy Dispersive X-ray Spectrometry, X-ray Diffraction, and so on, might also provide important qualitative and quantitative information of the foulant on the surface of different IEMs.

2.2 FOULING MITIGATION

As the characterization of fouling is very important for understanding the interaction between the foulants and the surface of the membranes used in RED, its control and mitigation is crucial to enhance the performance of the IEMs. Thus, fouling mitigation can reduce the adverse effects of fouling, providing an improved RED process efficiency. Mostly, fouling mitigation in IEMs is focused on membrane surface and its cleaning since it is a simple approach to reduce cost compared to preparing new membranes [89, 90]. The modification procedures may tune different properties of AEMs such as hydrophilicity, monovalent permselectivity, surface charge density, electrical conductivity and fouling resistance, among others.

Several surface modification procedures, as shown in **Figure 6**, have been applied to control and mitigate fouling phenomena, as well as render a monovalent membrane permselectivity [68, 91]. Different approaches such as surface polymerization (by UV-induced and oxidative self-polymerization) [92, 93], dip coating [30], electrodeposition [38], and layer-by-layer (LbL) deposition [94-97] can be found in literature. The chemical surface modification, adsorption, polymerization, ion implantation, solution casting, electric deposition, or plasma treatments are also considered either to modify the surface chemical structure or to add a new layer onto the AEM surface to induce an antifouling effect, improve the electrical conductivity, the permselectivity and the chemical, mechanical and dimensional stability [98-100]. These techniques purposely enhance the membrane hydrophilic properties.

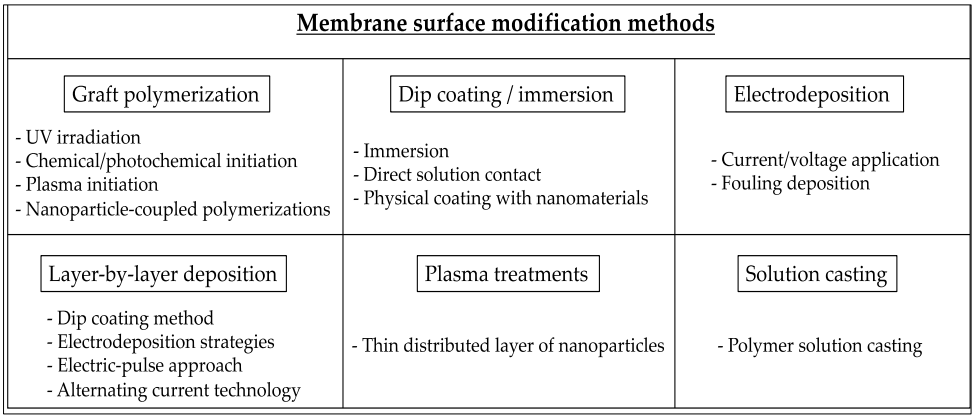

Figure 6 *Summary of predominant surface modification procedures[28]*

The different available and relevant ways to prepare modified AEMs with desired beneficial properties for RED systems, while also identifying the strengths and weaknesses of these membrane surface modification methods, are highlighted in the following subsections.

2.2.1. SURFACE POLYMERIZATION METHODS

UV induced surface graft polymerization (**Figure 7**) is effective technique to improving hydrophilicity of the membranes, leading to better antifouling resistance. It also allows for tuning the membrane surface properties with low processing costs and less or no damage to the bulk membrane material [93]. The possibility of improving the monovalent permselectivity of standard commercial AEMs through UV irradiation to reach values near those reported for commercial Neosepta and Selemion monovalent anion selective membranes has been reported in 2014 [26]. A negative coating layer containing the active polymer 2-acryloylamido-2-methylpropanesulfonic acid (AMPS), and the crosslinker N,N-methylenebis(acrylamide) (MBA) enhanced the membrane hydrophilicity and antifouling potential for RED applications. Losses in power density were reduced due to the induced antifouling characteristics. Besides, the authors proposed that thinner membranes (< 110 µm) might result in enhancing the net power density. Similar approach demonstrated that the AEMs electrochemical transport characteristics unchanged after creating a thin negatively charged hydrophilic and antifouling layer of urethane acrylate onto their surfaces. Controlling the UV radiation wavelength was essential to effecting the compactness and ion exchange capacities of the resulting modified membranes [101].

Another promising approach is the application of zwitterionic materials. Several methods such as photo-initiated, plasma-initiated, UV irradiation and graft polymerization polymerizes zwitterionic monomers [102], demonstrating the possibility of improving hydrophilicity as water contact angle is reduced, thereby, decreasing the adhesion of foulants. Industrially, the development and use of cheaper, stable, sustainable and eco-friendly modifying materials such as polyvinyl alcohol (PVA) and chitosan has also been considered to modify AEMs with designed beneficial properties [39, 103].

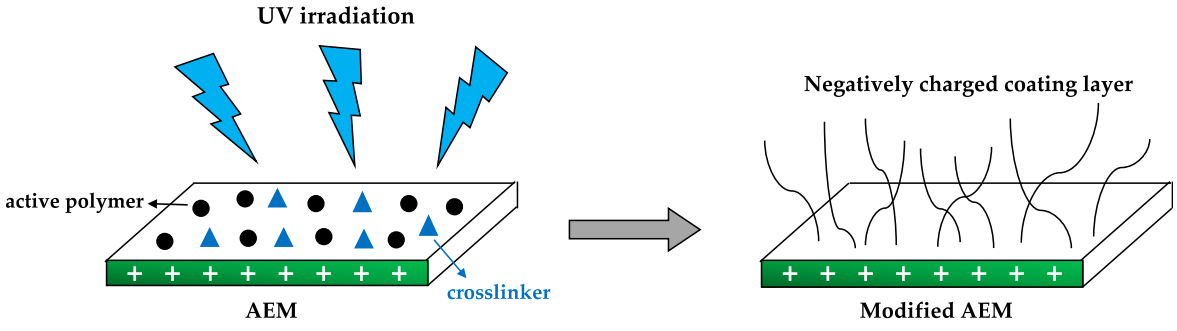

Figure 7 *Schematic description of UV induced graft polymerization of AEM*

2.2.2 DIP COATING METHODS

Dip coating, as demonstrated in **Figure 8**, involves immersing a membrane into a modifying agent solution to create an additional layer onto the surface at a controlled time [29, 76, 104]. The significance of the immersion time, modifier concentration, selection of the appropriate modifying agent to obtain a stable anionic polyelectrolyte layer on the surface of different Neosepta AEMs has been discussed elsewhere[105]. Irrespective of the modifying agent applied, similar tendencies for improved ion exchange capacity were achieved at optimum conditions. Other researchers employed high molecular mass anion active surfactants with alternating hydrophobic and hydrophilic groups as the modifier for the dip coating. For instance, this technique was applied to Ionics AEMs to enhance the fouling resistance of the membranes in the presence of SDBS as the model foulant [106]. Fouling was suppressed for 6 h when the concentration of SDBS was 30 ppm, though at 100 ppm, fouling was noticeable, signifying the importance of the impact of foulants concentration in natural streams on blue energy harvesting from RED.

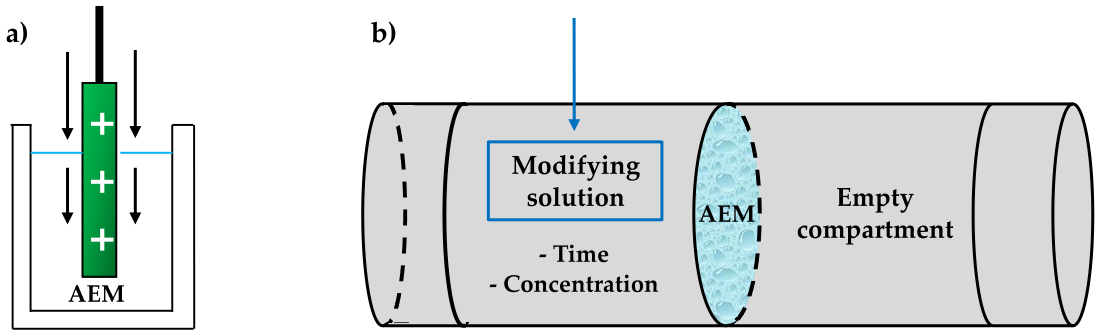

Figure 8 *Diagram representing dip coating set up fora AEM*

.

Recently, dip coating was also applied to create a negatively charged layer onto the surface of a Ralex AM-PES membrane, and Neosepta AMX. The immersion of the membrane into a polydopamine (PDA)-based solution was carried out vertically for 24 h, and demonstrated an improved rejection of divalent anions, while unaffecting the monovalent anion permselectivity after modification [30], which is essential for an enhanced RED process efficiency. The antibiofouling behavior of PDA-modified AEMs was improved when *Pseudomonas putida* was utilized as the model biofoulant [30]. Heterogeneous Ralex AEMs were also modified by direct contact (during 24 h) with poly(acrylic) acid (PAA)-based solutions, which represents the use of a non-toxic and stable modifying agent [59,60,[107, 108]. The authors reported an improved surface hydrophilicity and monovalent membrane permselectivity as a function of different concentrations of PAA which almost retained the membrane electro-resistance [29].

.

2.2.3 LAYER-BY-LAYER (LbL) STRATEGIES

The LbL-based technique (**Figure 9**) demonstrates a versatile and efficient way for improving RED performance, since it allows for tuning of the membrane properties, such as swelling, thickness or surface charge density [94, 95]. Optimizing the number of layers added to the membrane is important parameter for obtaining desirable properties. In other studies, alternative and repeated layers of

poly(sodium 4-styrene sulfonate), PSS polyanion and poly(allynamine hydrochloride), PAH polycation were deposited onto Neosepta AMX. The monovalent anion permselectivity improved after 15 layers of using a LbL deposition [67]. The authors attributed the improvement to an increase in the negative surface charge of the total excess area. However, the optimum antifouling potential was reached at 7 layers, where the lowest membrane water contact angle was achieved.

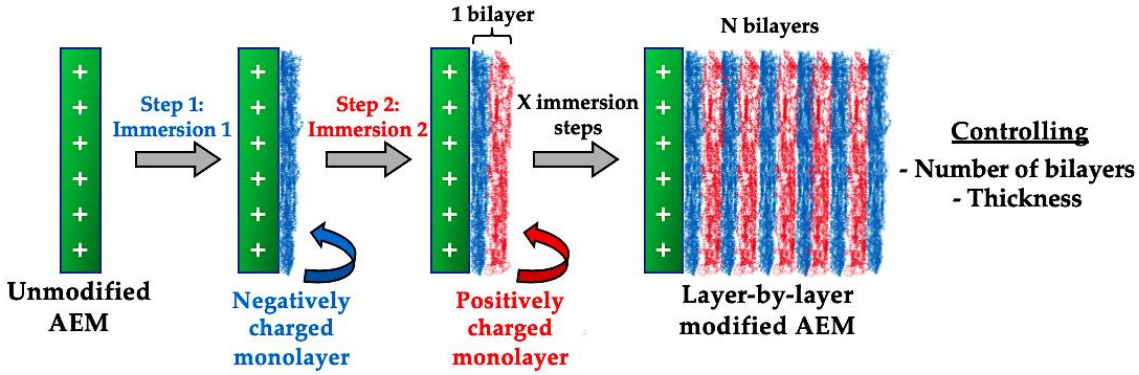

Figure 9 *Schematic representation of LBL approach*

Similarly, thin layers of PSS and poly(ethyleneimine) PEI cation were deposited on CJMA-2 standard AEM to tune the membrane properties [109]. The monovalent anion permselectivity enhanced at 7.5 bilayers and was comparable to commercial ACS monovalent selective membranes. The anti-organic fouling resistance improved by 38.4%. Due to the favorable characteristics of the prepared membrane, RED tests were carried out using $NaCl_{(aq)}$ and $Na_2SO_{4(aq)}$ employing HA as a model foulant. The net power density improved up to 17% and the energy conversion efficiency was improved.

Another interesting LBL approach applied in 2018 is electric-pulse LbL. Thus, N-O-sulfonic acid benzyl chitosan (NSBC) and hydroxypropyl trimethyl ammonium chloride chitosan (HACC) was coated onto one side of a commercial AEM [96]. This electric-pulse (provided by an electrochemical workstation) deposition technique activated both NSBC and HACC, leading to a tremendous adsorption capacity. A stable homogeneous multilayer with a relatively low surface electrical resistance was obtained at 7.5 bilayers.

An alternating current LbL (AC-LbL) technology has also been used at AC frequency of 50 Hz for AEM modification [95]. Thus, 7.5 bilayers of poly(4-styrenesulfonic acid-co-maleic acid) sodium salt and 2-hydroxypropyltrimethyl ammonium chloride chitosan were homogeneously deposited onto the surface of the membrane and then crosslinked using 1,4-bis(2′,3′-epoxypropyl) perfluoro-1-butane. The modified membrane attained desirable Cl^-/SO_4^{2-} permselectivity and antifouling properties, and stable operation for 96 h.

2.2.4 ELECTRODEPOSITION APPROACH

Electrodeposition, as represented in **Figure 10**, employs an electrical field to deposit a layer on AEM [104]. For instance, PEI was electrodeposited on home-made AEM to favor the migration of monovalent anions across the membrane, while hindering the transport of multivalent ions [110]. The Cl^-/SO_4^{2-} permselectivity increased from 0.79 to 4.27 due to a reduction in sulfate ion leakage rate from 39.6% to 19.4%. The modified membrane was stable at 70 h of continuous operation.

Moreover, 0.1-0.5 g/L of graphene oxide (GO) were electrodeposited on heterogeneous AEMs with the aid of supporting 0.01 M NaCl electrolyte [111]. At current density of 1-5 mA/cm^2, fouling resistance was improved in the presence of 150 mg/L SDBS used as a model foulant, since more hydrophilic surfaces with negative zeta potential were created on the membrane.

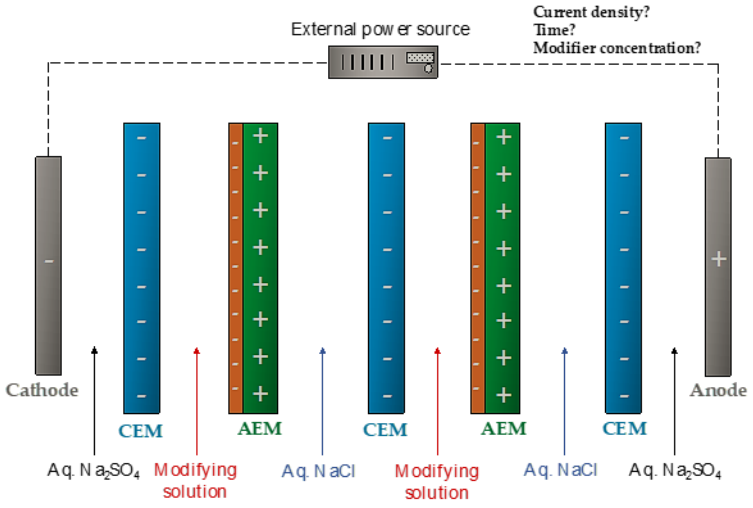

Figure 10 *Schematic representation of electrodeposition*

The same research group also studied the feasibility of combining electrodeposition and coating to incorporate a thin negatively charged and hydrophilic PDA layer onto the GO-AEMs (modified by electrodeposition) [112]. The authors demonstrated an extensive enhancement of the membrane stability with antifouling behavior in an electrodialysis apparatus operated at a constant voltage of 4 V for 20 h when a smoother and denser PDA/GO layer was incorporated. Furthermore, the possibility of increasing the performance of AEMs after membrane modification by electrodeposition using a polyelectrolyte containing different functional groups such as PSS and poly(sodium acrylate) (PAAS) was also clearly demonstrated in electrodialysis [113]. Their higher negative charge surface density enhanced the membrane antifouling behavior.

It is important to monitor and optimize the current/voltage applied to carry out the modifier electrodeposition, the amount of the deposited agent and its composition which determines the thickness of the modified AEM, to develop stable negative layers with hydrophilic, monovalent anion permselective and antifouling properties via electrodeposition.

2.2.5 FOULING DEPOSITION AND OTHER RELEVANT APPROACHES

Although fouling generally represents an undesirable phenomenon in the electro-membrane field, fouling deposition has been recently proposed and investigated to convert the adverse effect of fouling into useful tool to prepare permselective membranes, and antifouling [114]. For instance, Neosepta AMX AEMs were intentionally fouled with sulfonated poly(2,6-di-methyl-1,4-phenylene oxide) (SPPO) at constant current density levels of 10, 30 and 50 mA/cm^2 in electrodialysis system. The best membrane behavior was achieved at 10 mA/cm^2 at which a high Cl^-/SO_4^{2-} permselectivity coefficient of 52.44 was reached. That value was superior not only to that of an unmodified Neosepta AMX membrane, but also to a commercial monovalent anion permselective Neosepta ACS membrane. However, the authors claimed that a better understanding of the fouling mechanisms and the role of the fouling layer on membrane permselectivity are still required in this fouling deposition technology.

Other relevant membrane modification approaches which include the use of nanomaterials, solution casting have also been used to modify AEM to improve monovalent permselectivity, tune roughness and morphology, and enhance antifouling characteristics [66]. For example, a commercial polyethylene AEM was modified by physical coating using sulfonated poly(2,6-dimethyl-1,4-phenylene oxide) (SPPO) and two nanomaterials of different geometry with optimized loadings (oxidized multi-walled carbon nanotubes, CNTs-COO-, or sulfonated iron oxide NPs, Fe_2O_3-SO_4^{2-}). The hydrophilicity and homogeneity of the modified AEM improved without compromising the membrane electro-resistance. Thus, the antifouling potential enhanced by 45%, using sodium dodecyl sulfate (SDS) as the model foulant [115].

3. MATERIALS AND METHODS

3.1 MEMBRANE PREPARATION

Commercial heterogeneous Ralex-AEMs (**Figure 11**, MEGA, Czech Republic) were modified with different PAA-based solutions (from 1 g/L to 5 g/L) for 24 h, while monitoring the pH and conductivity.

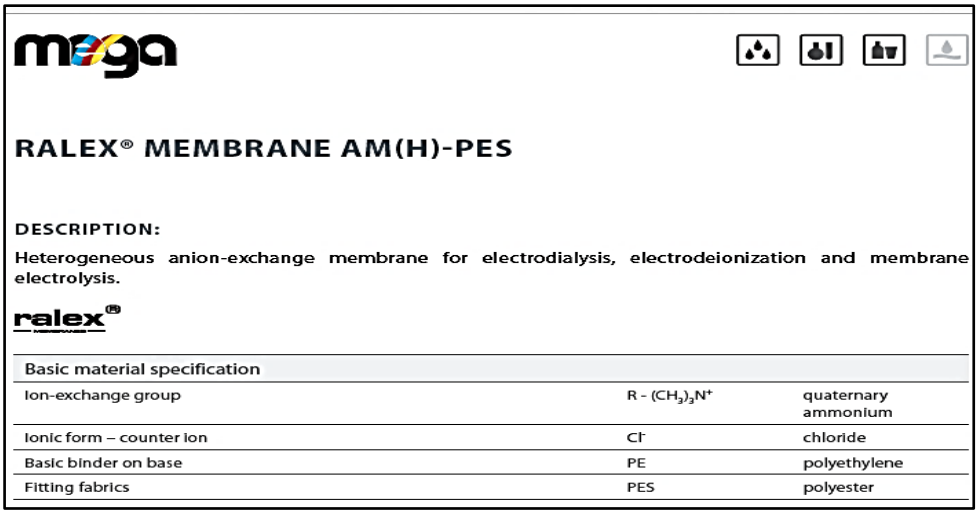

RALEX® MEMBRANE AM(H)-PES

DESCRIPTION:

Heterogeneous anion-exchange membrane for electrodialysis, electrodeionization and membrane electrolysis.

ralex®

Basic material specification		
Ion-exchange group	R - $(CH_3)_3N^+$	quaternary ammonium
Ionic form – counter ion	Cl^-	chloride
Basic binder on base	PE	polyethylene
Fitting fabrics	PES	polyester

Figure 11 *Manufacturer's description of the Ralex-AEM*

The set-up of the modification included two compartments diffusion cell. We dissolved 14.04 g of TrizmaHCl and 1.34 g of Trizmabase in 1 L of demineralized water to obtain 0.1 M Trizma® aqueous buffer solution of pH 7.2 at 25 ℃. The PAA (1 g to 5 g each) was dissolved in 1 L of the 0.1 M Trizma® solution to induce a negatively charged PAA. The AEM was immersed in the PAA solution, as presented in **Figure 12**, for 24 h to introduce the negative PAA monolayer onto the membrane surface. This process is called functionalization. After functionalization, the modified membrane was brought into contact with a fresh 0.1 M Trizma® for 24 h to ensure the effective removal of excess PAA.

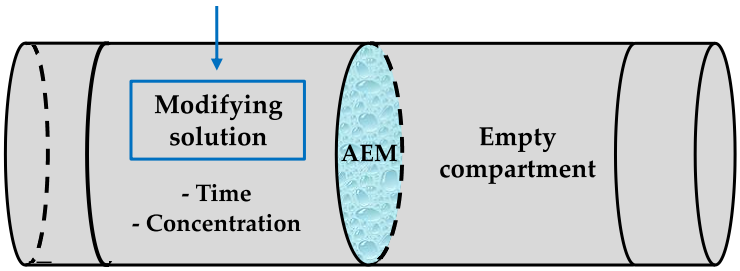

Figure 12 *Two compartment diffusion cell used for membrane modification*

The resulting PAA modified membranes (PAA-AEMs) were totally immersed and kept in deionized water before characterization and use. The modification parameters, conditions and classification of the membranes are shown in **Table 1**.

Table 1 AEMs under study: classification and characteristics

Membrane list	Modification type	PAA concentration (g/L)	Nomenclature
(1)	Unmodified	-	Unmodified
(2)	Monolayer/one	1	One side 1 g/L PAA
(3)	Monolayer/one	3	One side 3 g/L PAA
(4)	Monolayer/both	3	Both sides 3 g/L PAA
(5)	Monolayer/one	5	One side 5 g/L PAA

3.2. PHYSICOCHEMICAL CHARACTERIZATION OF MEMBRRANE

3.2.1 WATER CONTACT ANGLE (WCA) AN WATER UPTAKE (WU)

Initially, the membranes were dried at 35 ℃ for 24 h. A goniometer (CAM 100, KSV Instruments Ltd.) was used to evaluate the water contact angle corresponding to the surface hydrophilicity or hydrophobicity. In the experiment, deionized water droplet (**Figure 13**) was provided by means of a syringe onto the membrane surface, where at least 4 surface points were taken into consideration to reach an averaged contact angle value in each case, including the standard deviation.

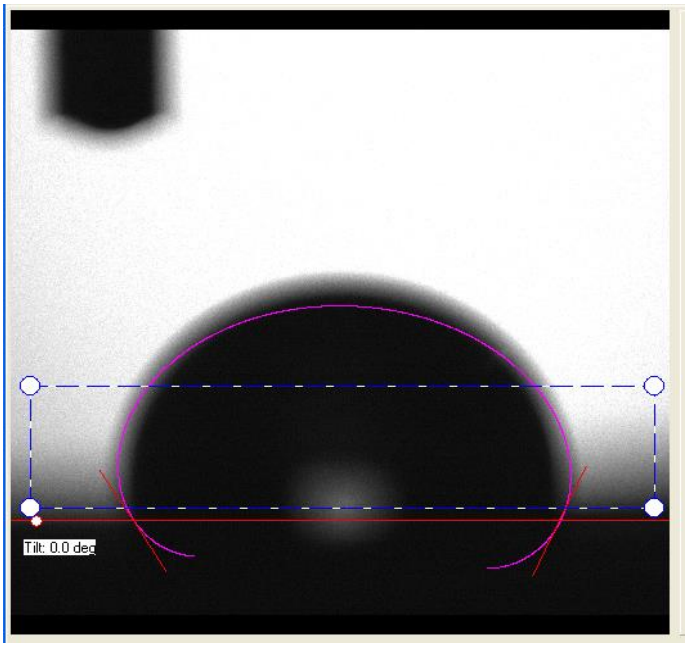

Figure 13 *Image of water droplet on the membrane surface for contact angle measurement*

The WU of the prepared AEMs was also evaluated. Firstly, the AEMs were dried at 35℃ for 24 h. Keeping the membranes in a desiccator for 1 day removed traces of water. Finally, the dried membranes were weighed (m_{dry}) and totally immersed in deionized water for 24 h. The mass of the corresponding wet AEMs (m_{wet}) was measured, after removing the excess of water from membrane surface with a tissue paper. The %WU was then calculated as depicted in **Eqn. 24**.

$$WU\ (\%) = \frac{m_{wet} - m_{dry}}{m_{dry}} \times 100 \tag{24}$$

The swelling effect was also evaluated by measuring the thickness (using Elcometer 124 Thickness gauge) and diameter of the dried and wet AEMs.

3.2.2 ION EXCHANGE CAPCITY (IEC) AND FIXED CHARGE DENSITY

The IEC represents the amount of fixed charged groups per unit weight of dry polymer in the prepared AEMs. Two methods namely the Mohr titration method, and UV-VIS spectrophotometric method [116, 117] were adapted.

Regarding the Mohr titration method, already weighed wet AEM was immersed in 0.4 M NaCl aqueous solution for 24 h. The AEM was removed from the NaCl solution, rinsed with demineralized water and placed in 0.2 M Na_2SO_4 aqueous solution for 6 h to replace the Cl^- on the AEM surface with SO_4^{2-} from the solution. The resulting solution containing the released Cl^- was finally titrated against 0.1 M $AgNO_{3(aq)}$, adding two drops of 0.1 M potassium chromate (K_2CrO_4) indicator. The endpoint was visually determined when the yellowish color of the indicator changed to reddish-brown. The IEC (in mmol/g) of the AEM was calculated according to **Eqn. 25**.

$$IEC\ (mmol/g_{dry}) = \frac{V_{AgNO_3} \times N_{AgNO_3}}{m_{dry}} \quad (25)$$

Concerning the UV-VIS spectrophotometric method, AEM was immersed in 1 M KNO_3 aqueous solution for 24 h. The AEM was removed from the KNO_3 solution, rinsed with demineralized water and immersed in 0.1 M NaCl for 12 h to replace the NO_3^- on the membrane surface with Cl^- from the NaCl solution. We measured the absorbance of the released NO_3^- using a UV-VIS spectrophotometer (Thermo Scientific Evolution 201) set at 300 nm wavelength, and calculated the NO_3^- concentration from the absorbance, considering a prepared calibration curve. The IEC was determined by dividing the NO_3^- mole by the dry weight of the AEM.

The membrane fixed charge density (CD_{fix}), which represents the concentration of fixed charge groups per unit volume of water in the membrane under study, was estimated as shown in **Eqn. 26**.

$$CD_{fix} = \frac{IEC}{WU.} \quad (26)$$

3.2.3 FOURIER ATTENUATED ATOMIC FORCE MICROSCOPY (ATR-FTIR)

The ATR-FTIR detected the functional groups at the dried membrane surface employing a Spectrum Two FT-IR Spectrometer (PerkinElmer) in transmittance mode. Each membrane under steady was scanned considering wave number of 4000 cm^{-1}- 400 cm^{-1}. At least three points from different positions of the membrane surface were analyzed to ensure spectral reproducibility in each case. The spectra of each modified membrane were compared with the unmodified to confirm the presence of the PAA monolayer.

3.3 MEMBRANE ELECTROCHEMICAL CHARACTERIZATION

The modified and unmodified AEMs were electrochemically characterized via linear sweep voltammetry (LSV), cyclic voltammetry (CV), and electrochemical impedance spectroscopy(EIS).

3.3.1 LINEAR SWEEP VOLTAMMETRY (LSV), AND CYCLIC VOLTAMMETRY (CV)

The set-up used for the voltammetry measurements is presented in **Figure 14**. Two-compartments diffusion cell was used to study the effects of each electrodes and their relative position to reach ideal resistor performance. Therefore, copper (Cu), graphite (C) and silver (Ag) rods were the electrodes selected in this study. The working electrode and the counter electrode were inserted in the receiver and feed compartments respectively. The feed compartment was filled with 1 g/L $NaCl_{(aq)}$ + 0.1 g/L $Na_2SO_{4(aq)}$ +25 ppm HA (named as LCC), whereas 30 g/L NaCl (HCC) representing sea water was utilized at the receiver side. Initially the LSV was conducted from -0.6 V to 0.6 V to provide a gist on the

I-V behavior of the electrodes. The CV was then performed from -0.6 V to 0.6 V at scan rate of 200 mV/s.

Figure 14 *Two compartment diffusion cell used for electrochemical characterization of the membrane*

The potential was controlled by utilizing a potentiostat/galvanostat (Ivium Technologies, Netherlands). Three repeated scans were carried out in all tests to study membrane and diffusion stability. In this context, I-V responses obtained from the voltammogram were related to the overall transport of ions across the corresponding AEM under study. Additionally, the effect of the nature of the co-ion was investigated at the current obtained at the maximum applied voltage (0.6 V). In that case, four different feed aqueous solutions of KCl + Na_2SO_4, KCl + K_2SO_4, NaCl + Na_2SO_4, and LiCl + Na_2SO_4 with the same molar concentration (*i.e.,* 0.017 M + 0.0007 M) were evaluated.

3.3.2 ELECTROCHEMICAL IMPEDANCE SPECTROSCOPY(EIS)

The EIS was conducted using a redox flow cell set-up designed by Østedgaard-Munck et al [118, 119]. In this respect, the membrane electro-resistance was the key parameter to be analyzed. The set-up image for the EIS is portrayed in **Figure 15**. The geometric active area of the cell is 6.25 cm^2. One stainless steel end plate is placed as a final element at the end of each cell side. The end plates are electrically insulated from gold plate-based current collectors by using a Viton sheet. Graphite blocks act as electrodes, which are intentionally designed with an interdigitated flow pattern based on 12 channels with a dimension of 25 mm x 25 mm x 2 mm. Also, two Teflon gaskets were located between the electrodes and the membrane to ensure the correct adjustment of the key element of the system.

Two feed streams of 0.5 M $NaCl_{(aq)}$ were supplied in co-flow mode to the cell at 20 mL/min by using a peristaltic pump (Masterflex, Cole Palmer). The cell was tightened diagonally at 3.0 Nm torque using a torque wrench, enabling optimum contact between the electrodes of the flow cell and the membrane.

Employing the Ivium potentiostat as mentioned above, the EIS was performed at room temperature, constant voltage of 50 mV, 0.1 V amplitude, and frequency range of 0.5 MHz to 100 Hz. The EIS measurements were repeated to allow for the estimation of the averaged membrane electro-resistance, considering the blank solution.

Figure 15 *Set-up image of the redox flow cell and the peristaltic pump used for the EIS measurements*

The data was fitted through equivalent circuit analysis (EC) to quantify R_m, R_{EDL} and R_{DBL}, as already presented in **Figure 4**. Due to the high frequency range used in this study, we expect that the DBL effect should be lower than the one related to the membrane resistance, even though it has also been assessed for the sake of clarity. Therefore, we focused mainly on the R_m, though the R_{EDL} and R_{DBL} will be considered. Moreover, 0.5 M $NaCl_{(aq)}$, 0.5 M $KCl_{(aq)}$ and 0.5 M $LiCl_{(aq)}$ were also considered to evaluate the effect of changing the co-ion on the membrane electro-resistance.

3.4 MASS TRANSPORT EXPERIMENTS

Diffusion test helps to monitor the transport of ions through the AEM in the absence or presence of foulants. In this respect, the counter-ion permselectivity and fouling behavior of the prepared AEM was evaluated in the absence/presence of HA. The diffusion cell experiment was conducted with the same equipment shown in **Figure 14**. However, in the mass transport tests (**Figure 16**), no electrodes were inserted, since the driving force was the salinity gradient between the receiver and the feed chambers. Thus, the feed and the receiver compartments were filled with 200 mL of model streams of low (*i.e.,* river water) and high (*i.e.,* seawater) salt concentrations, respectively, while 25 ppm of HA (Fluka, Ign. residue: ~20 %) was introduced in the feed solution in several experiments as model organic foulant to evaluate fouling behavior. Samples were taken at 0, 2, 4, 7, and 24 h period.

The pH, and ionic conductivity of samples taken from the feed and receiver chamber were measured. The Na^+, SO_4^{2-} and Cl^- ions $^-$ in each feed and receiver were also determined via inductively coupled plasma spectroscopy (ICPS) which determined the amount of Na and S. The amount of SO_4^{2-} was calculated based on the quantity of S measure, whereas the concentration of Cl^- was calculated using charge balance. In the presence of HA, the absorbance of feed and receiver solutions was studied by a UV-VIS spectrophotometer (Thermo Scientific Evolution 201) set at 280 nm wavelength to demonstrate that HA is not permeating the membrane from the feed to receiver compartment.

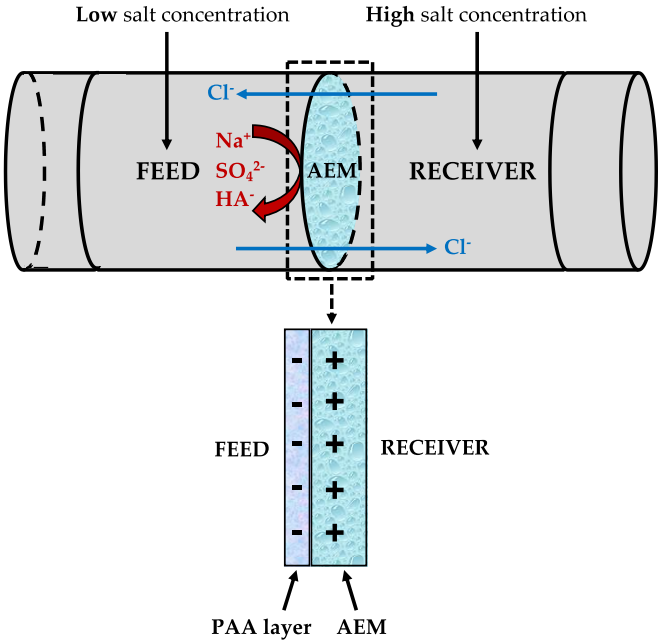

Figure 16 *Set-up image for transport studies, including the graphical aspect of the modified AEM*

3.5 REPETITIVE FOULING AND CLEANING

Cleaning is an important treatment process required for removing attached foulants which are present on the surface of the AEMs. Different cleaning solutions such as NaOH, HCl, and other combinations are employed depending on the type of foulant, whether organic, inorganic, colloidal or biological [21, 87, 120]. In this study, we evaluated the cleaning effect of NaOH on the resistances of the unmodified AEM and the one side 3 g/L PAA after fouling. NaOH has been mentioned to be effective for organic foulant removal [33]. Therefore, it was selected for this study since HA is an organic foulant.

Prior to fouling, the resistance of the unfouled membranes were determined via EIS. 500 ppm of HA was used to foul the membranes for 10 mins in the same redox flow cell used to study EIS measurements. The resistance of the fouled membrane was then evaluated. The fouled membrane in the flow cell was cleaned with 0.1 M NaOH at a flowrate of 20 mL/min for 3 min, followed by water rinsing for 1 min at the same flowrate. Finally, the resistance of the cleaned membrane was determined. This procedure was conducted in three cycles to evaluate the resistance effect of fouling and cleaning.

4. RESULTS AND DISCUSSION

This part of the thesis presents and discusses the results obtained from the physicochemical characterizations, electrochemical characterizations of the AEMs, mass transport studies, fouling and cleaning. The results are mainly focused on the alterations of the membrane properties after modification, related to the hydrophilicity, ion exchange capacity, sulfate rejection, and electrical resistance.

4.1 CONTACT ANGLE, WATER UPTAKE, AND SWELLING DEGREE (SD)

The surface hydrophilicity of the unmodified and the one-side PAA modified membranes was evaluated by measuring the WCA. The unmodified membrane recorded the highest WCA, denoting lowest hydrophilicity. Regarding the one side modified membranes, the lowest hydrophilicity (15%) was recorded in the one side 1 g/L PAA. Hydrophilic properties were improved when increasing the PAA concentration up to 3 g/L, but further concentration increment to 5 g/L involved a loss of hydrophilicity, as shown in **Figure 17**. Thus, the optimum hydrophilicity was attained at 3 g/L, representing 31 % reduction in the WCA. The lack of hydrophilicity enhancement in the 5 g/L might be due to surface saturation at higher PAA concentrations. It is worth to highlight that different positions on the surface of the dried membranes under investigation were considered to reach averaged contact angle values.

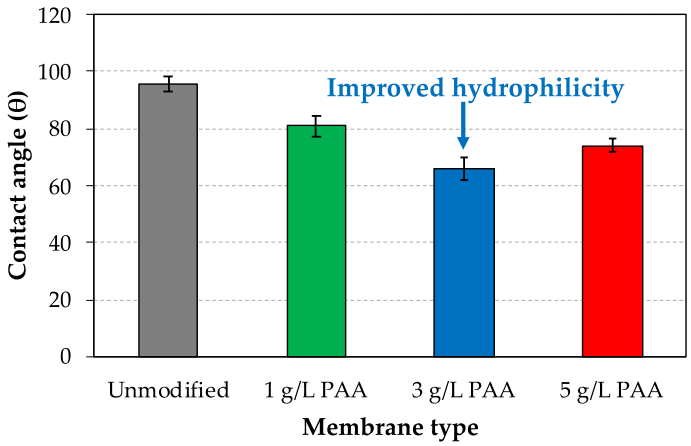

Figure 17 *Hydrophilicity analysis: contact angle data*

Table 2 presents the results of the WU, and SD. Generally, the modified AEMs demonstrated higher WU compared to the unmodified membrane, denoting the higher hydrophilic properties of the membranes. Considering the standard deviations, the changes in the PAA concentration did not change the WU values appreciably, signifying comparable water absorption properties of the PAA-modified AEMs.

Membrane swelling is also an essential parameter that may limit the performance of RED. The SD increases the membrane thickness which may increase its electrical resistance, leading to reduced

power output from RED. Even though swelling degree is often measured as water uptake in literature [116, 121], it is important to point out here that SD should also be quantified in terms of membrane dimensional changes (e.g., thickness and diameter). The thickness of both dried and wet PAA-AEM was slightly higher than the unmodified membrane, as observed in the WU. Compared to their dry condition, appreciable changes in the thickness was noticed in all membranes under investigation after swelling, representing 36-38% increment. Similar trend was attained in the diameter of the wet and dried membranes though increased by 5 %. The 36-38% increment in thickness demonstrates the need to control the potential change in membrane thickness for improved RED performance, since higher thickness might result in increased membrane electro-resistance and lower obtainable net power density. Controlling the dimensions of AEMs is essential for optimizing the membrane design and operating conditions for RED applications.

Table 2 WU, thickness and diameter of dry and wet AEMs

Membrane type	WU (%)	Thickness wet (μm)	Thickness dry (μm)	Diameter wet (mm)	Diameter dry (mm)
(1) Unmodified	59.0 ± 1.8	643.3 ± 5.8	472.7 ± 2.3	45.7 ± 0.6	43.3 ± 1.2
(2) One side 1 g/L PAA	67.4 ± 6.0	664.0 ± 0.0	487.7 ± 4.0	45.0 ± 1.7	44.8 ± 2.0
(3) One side 3 g/L PAA	62.7 ± 3.8	654.7 ± 4.6	473.3 ± 2.3	47.3 ± 1.2	44.8 ± 0.8
(4) Both sides 3 g/L PAA	61.5 ± 0.9	650.0 ± 20.4	473.7 ± 6.0	47.7 ± 1.5	45.5 ± 0.5
(5) One side 5 g/L PAA	63.3 ± 5.0	654.8 ± 21.3	476.0 ± 5.3	47.3 ± 0.6	45.3 ± 0.6

4.2 ION EXCHANGE CAPACITY, AND FIXED CHARGE DENSITY

The IEC is one of the important properties of AEM since they denote how the membrane can allow ion exchange and transfer across the membrane. Membrane composition influences the IEC due to the different fixed functional groups, which can be divided into weak and strong ion-exchangers according to their dissociation constants [117]. The Mohr's method and spectrophotometric method were employed for the IEC. As displayed in **Table 3**, IECs from 0.3 to 0.95 mmol/g were obtained using the Mohr's method. The unmodified membrane achieved the highest IEC (0.95 mmol/g) compared with all the PAA-AEMs. This implies that as the concentration of PAA increases from 1 g/L to 5 g/L, a stronger repulsion between the PAA layer and the SO_4^{2-} occurs, hence, decreasing the ability of SO_4^{2-} to replace Cl^- on the PAA-AEMs.

On the contrary, we determined IEC of 1.3 to 1.8 mmol/g using the spectrophotometric measurements. The modified AEMs attained higher IEC than the unmodified, even though the effects of PAA concentration seemed negligible at higher concentrations. This shows that the replacing the NO_3^- on the PAA-AEMs with Cl^- was greater than that observed in the Mohr's method, considering Cl^- and SO_4^{2-}. The results show that IEC values depend on the method applied, which suggests that selecting the most appropriate analytical technique to evaluate IEC in modified membranes is crucial. The difference in the Mohr's and the spectrophotometric methods agrees with other studies on different IEC methods

for homogeneous and heterogeneous AEMs [117]. The authors reported that the Mohr's method generally involves higher errors due to the difficulty to determine the final equivalent point, and the pH condition that must be controlled.

Table 3 Ion exchange capacity and fixed charge density of the studied AEMs

Membrane type	IEC[a] (mmol/g)	IEC[b] (mmol/g)	CD_{fix}[a] (mmol/g)	CD_{fix}[b] (mmol/g)
(1) Unmodified	0.949 ± 0.18	1.369 ± 0.05	1.605 ± 0.25	2.321 ± 0.08
(2) One side 1 g/L PAA	0.681 ± 0.03	1.625 ± 0.05	1.017 ± 0.14	2.413 ± 0.08
(3) One side 3 g/L PAA	0.433 ± 0.01	1.751 ± 0.05	0.692 ± 0.05	2.793 ± 0.08
(4) Both sides 3 g/L PAA	0.378 ± 0.01	1.751 ± 0.05	0.614 ± 0.02	2.847 ± 0.08
(5) One side 5 g/L PAA	0.352 ± 0.02	1.760 ± 0.05	0.560 ± 0.08	2.779 ± 0.08

[a] Titration method; [b] Spectrophotometric method

They compared Mohr's method, and spectrophotometric respective values of 2.32± 0.08 and 2.45± 0.05 with elemental analysis value of 2.61± 0.03. The authors reported that the spectrophotometric method was closer to the elemental analysis, indicating that the spectrophotometric results are more accurate than the Mohr's method. As a result, we would like to recommend spectrophotometric approach to determine the IEC of surface modified AEMs for a higher accuracy.

The CD_{fix} is influenced by both the IEC and WU. Since different IECs values were observed as a function of the method used, the CD_{fix} followed similar trend in the IEC.

4.3 FOURIER TRANSFORM INFRARED SPECTROSCOPY

The detection of the functional groups on the membranes surface under study is shown in the ATR-FTIR spectra of **Figure 18**. Similar ATR-FTIR spectra can be observed for all the membranes, indicating that the PAA concentrations did not produce significant changes in FTIR spectra. This suggests the absence of chemical reactions between the PAA and the membrane, implying that the attachment was electrostatic. Since PAA is not covalently bonded to the membrane, the amount of PAA before membrane washing with Trizma® solution is expected to be higher and, therefore, FTIR signals for the PAA-AEMs should be stronger, helping to easily identify the expectable contribution of PAA to the FTIR spectra

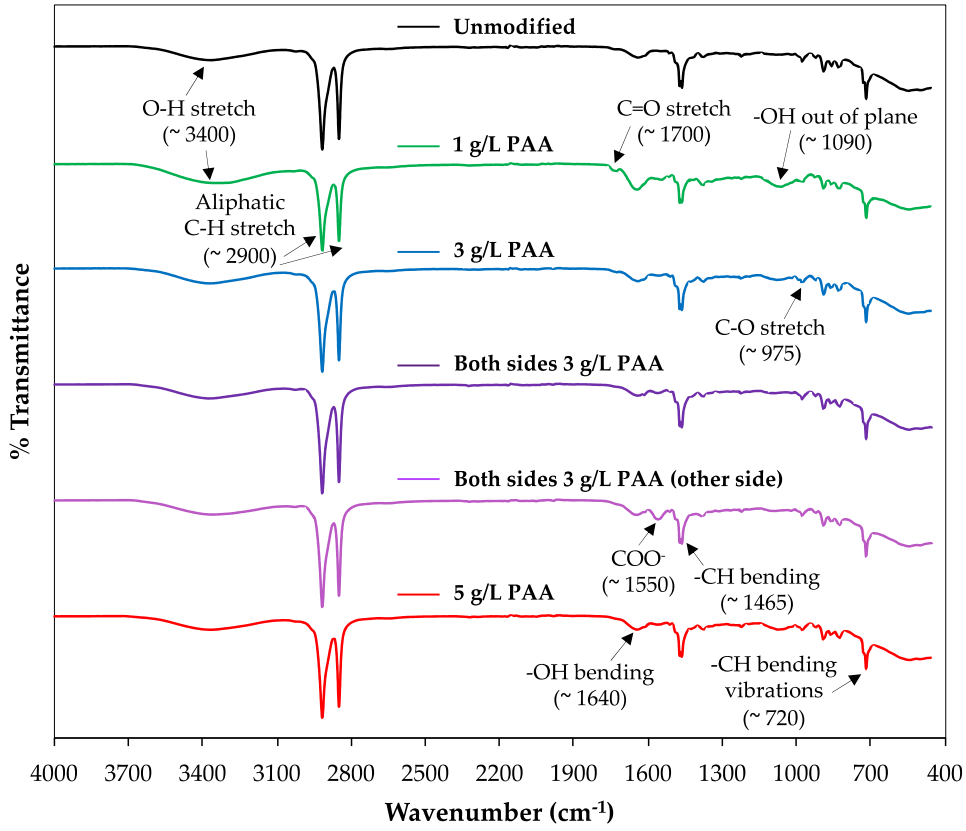

Figure 18 *ATR-FTIR spectra of unmodified and PAA-modified AEMs*

However, the washing step was essential because the goal was to remove the loosely attached PAA to avoid their release during experimental studies, while ensuring membrane stability. Also, similar functional groups present in both the Ralex membrane and PAA causes additional difficulties in accessing the presence of PAA. Thus, the different bands observed in the spectra correspond to the polyester fabric in the Ralex AEM, and the PAA on the membrane surface. The first band at ~3400 cm^{-1} is related to the O-H stretch of the carboxylic group present in both the polyester and PAA, whilst the peaks around 2900 cm^{-1} are associated with the C-H stretch of the two substances, corresponding to -CH_2 and -CH_3 groups. At ~1700 cm^{-1}, the C=O stretch can also be identified, which relates to polyester of the Ralex AEM and the carboxylic group of the PAA. Moreover, the sharp peaks around 1640 and 1465 cm^{-1} correspond to PAA and polyester as -OH and -CH bendings, respectively [122, 123]. At 1090 cm^{-1}, the peak might be either associated to carboxylic group -OH out of plane or O=C-O-C stretching of the main polymer of the membrane [123, 124]. This band is more visible in the modified membranes compared to the unmodified AEMs, which the authors relate to the inclusion of an additional -OH group during surface modification with PAA. The peak observed at 975 cm^{-1} assigned to the glycol C-O stretch [124], and the C=C stretching related to the benzene ring of the polyester. Moreover, -CH bending vibrations signal was also identified at 720 cm^{-1} [125]. Since the pH of the solution during modification was higher than 6.4, the dissociation of COOH into COO^- and H^+ is clearly presented in the PAA-AEMs at ~1550 cm^{-1} [126], indicating the presence of PAA on the modified membrane surfaces. The ATR-FTIR spectra shows that the polyester-based AEMs was still stable after the surface modification.

4.4 ELECTROCHEMICAL CHARACTERIZATION: CV

The AEMs were initially characterized electrochemically via CV. The optimum conditions were determined by evaluating the influence of type of electrodes, relative electrodes position in the diffusion cell, and the presence of HA. Cu, graphite (C) and Ag were the electrodes we investigated. The Cu electrodes exhibited oxidative problems and low current responses at potential window of -0.6 V to 0.6 V. The application of graphite electrodes in both compartments resulted in poor electrochemical responses associated with low conductivity. The combination of a graphite electrode with a silver rod improved the membrane behavior related to the current-voltage response. However, Ag-Ag electrodes allowed us to reach almost ideal resistor performance due to the high stability and conductivity of this material in aqueous solutions. Essentially, the Ag-Ag electrodes reached zero current at zero voltage (**Figure 19**), crucial for electro-membrane characterization. Moreover, HA did not influence the current voltage profile, signifying the negligible impact on the overall transport of ions across the membrane. Therefore, the Ag-Ag combination was selected for the CV. The effect of PAA concentration on the current-voltage behavior was also investigated. The influence on the current-voltage profiles for all membranes was small. Thus, the PAA-AEMs attained similar current signals, which is related to a comparable overall transport of ions through the corresponding modified membranes.

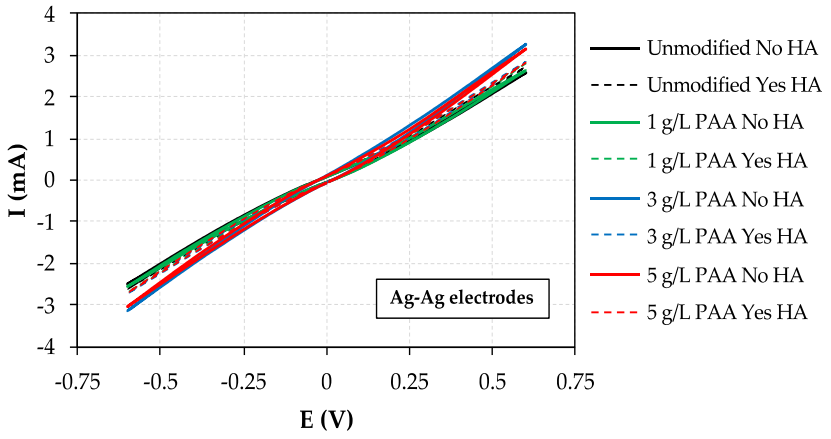

Figure 19 *Cyclic voltammogram of unmodified and PAA modified membranes*

The best electrochemical membrane performance was observed in the 3 g/L and 5 g/L of PAA, since they reached higher currents even at lowest voltage of -0.6 V. However, the 3 g/L and 5 g/L achieved a low overall current-voltage response in the presence of 25 ppm HA in the feed chamber. This effect may be due to some interactions between the HA and the PAA which hindered the overall transport of ionic species through the membrane under investigation. This issue was further investigated via mass transport experiments. The results of the CV were confirmed by LSV analysis (see **Appendix A1**).

The influence of co-ions in the feed stream was also evaluated, considering the unmodified, 3 g/L PAA and 5 g/L PAA modified AEMs, at maximum applied voltage (**Table 4**). Although the Donnan exclusion of the co-ions Na^+, K^+ and Li^+ is expected to be highly efficient to induce a lower impact on the Cl^- and

SO_4^{2-} counterions transport across the different AEMs, a clear trend ionic transport was noticed. Thus, the electrolyte "leakage" and conductivities follow the order KCl > NaCl > LiCl , which resulted in highest current in KCl but lowest in LiCl because their transport is related to their corresponding current achieved. This obvious trend is due to the decreasing hydrated radii in the trend $Li^+ > Na^+ > K^+$, as well as the differences in the diffusivity coefficients of KCl, NaCl and LiCl. This behavior was noted whether the membranes were modified or not, denoting that the nature of the co-ion involved in the system is not affecting the monovalent permselectivity of the prepared membranes, which is crucial for an improved performance in RED applications. Therefore, we can conclude that the nature of the co-ion is not of great interest, from a membrane permselective perspective.

Table 4. Currents obtained at the maximum applied voltage of 0.6 V

Membrane type	Feed solution	Current (mA) at 0.6 V
(1) Unmodified	KCl + Na_2SO_4	3.2
	KCl + K_2SO_4	3.5
	NaCl + Na_2SO_4	2.7
	LiCl + Na_2SO_4	2.6
(3) One side 3 g/L PAA	KCl + Na_2SO_4	3.3
	KCl + K_2SO_4	3.4
	NaCl + Na_2SO_4	3.2
	LiCl + Na_2SO_4	2.8
(3) One side 5 g/L PAA	KCl + Na_2SO_4	3.4
	KCl + K_2SO_4	3.8
	NaCl + Na_2SO_4	3.2
	LiCl + Na_2SO_4	3.0

4.5 ELECTROCHEMICAL CHARACTERIZATION: EIS

The EIS was performed in frequency range of 0.5 MHz to 100 Hz to focus mainly on the R_m though the R_{EDL}, R_{DBL} will also be discussed for clarity. The EIS results was fitted by equivalent circuit analysis (EC) incorporated in the Ivium potentiated software. Considering series and parallel combination of a resistor (R) and two capacitors (C) as aforementioned in **Figure 4**, these combinations produced the least error function, and deviations. At higher frequencies (*i.e.,* ≥ 10 kHz), the real impedance at zero phase shift (ϕ) represented R_m, considering the blank solution. The evolution of the experimentally measured impedance and phase shift of the unmodified AEM as a function of frequency range is represented by the Bode's plot (**Figure 20 a**). From the fitting, the R_m, R_{EDL}, and R_{DBL} of the unmodified membrane was 5.01 ± 0.52 Ω·cm^2 (at 1.7x10^4 Hz), 1.83 ± 0.23 Ω·cm^2 (at 500 Hz to <1.7x10^4 Hz), and 0.74 ± 0.15 (at 100-500 Hz Ω·cm^2), sequentially. The magnitude of the R_m relative to the R_{EDL} and R_{DBL} denotes that the limitation of ions transfers is higher in the membrane. Nevertheless, if the frequencies were operated in very low regimes, the effect of the EDL and DBL could be higher. The resistances measured in this

study is coherent with those measured in other work in the range of 5 Ω·cm^2 to 7 Ω·cm^2 [127]. The ohmic and non ohmic resistances using 30 g/L NaCl at the receiver compartment and 1 g/L NaCl + 0.1 g/L Na_2SO_4 at the feed compartment was also evaluated (see **Appendix A2**).

In **Figure 20**, the Nyquist's and Bode's plots show the evolution of the real (Z') and imaginary (Z'') impedances. In this work, a very small part of the semicircle in Nyquist plots appears due to the higher but shorter frequency range of 0.5 MHz to 100 Hz considered to avoid possible salt accumulation in the graphite blocks of the electrochemical cell, and the predominance of charge transfer restrictions at low frequencies. The very small error function is enough for the accuracy of the fitting.

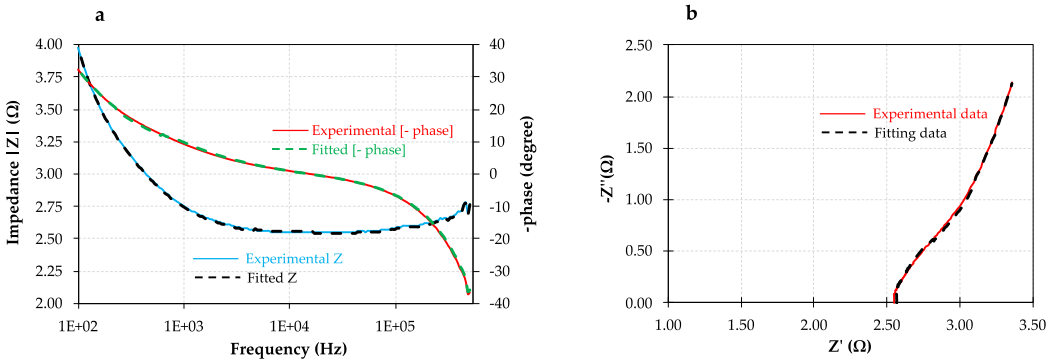

Figure 20 *EIS results represented in Bode plot(a), and Nyquist plot(b)*

The small increment in R_m observed in the PAA-AEMs (**Table 5**) might be associated with the additional PAA layer on the membrane, which increased the membrane thickness. Also, the R_{EDL} measured in the PAA-AEMs were closer to the unmodified (1.8 Ω·cm^2). They differed by 8% maximum and some of the modified membranes even achieved 15% lower R_{EDL} than the pristine. Therefore, these small differences imply that the addition of PAA monolayers with different modifying concentrations onto heterogeneous AEM did not compromise the electrical conductivity and the electrical resistances of the PAA-AEMs. Thus, the results obtained suggest that the PAA is distributed uniformly on the membrane surface, which may lead to a reduced disorderliness and surface heterogeneity, as well as enhanced charge transfers. This is eminent for enhancing the obtainable net power density from RED. Although the R_{DBL} values of up to 0.9 Ω·cm^2 is appreciable in the 100-500 Hz, it can be reduced by optimizing the hydrodynamic flow such as either increasing the flow rate or inducing turbulence [42].

The results from the EIS agree strongly with those we obtained from the direct current method (**Appendix A3**), and the change in the electrical resistances of modified AEMs are consistent with other studies [30, 106, 128] (see **Appendix A4**). The EDL is in nanometer scale, hence flow rate might not have appreciable impact on it generally, just as it does not influence the R_m substantially, employing 0.5M NaCl [42], depending on the membrane.

Table 5 Electrochemical parameters obtained from equivalent circuit fitting to experimental data (using 0.5 M NaCl as the electrolyte)

Membrane type	R_M ($\Omega \cdot cm^2$)	R_{EDL} ($\Omega \cdot cm^2$)	R_{DBL} ($\Omega \cdot cm^2$)	C_{EDL} (μF)	C_{DBL} (μF)	X^2 error function
(1) Unmodified	5.01 ± 0.52	1.83 ± 0.23	0.74 ± 0.15	115 ± 16	46 ± 10	0.0023
(2) One side 1 g/L PAA	5.14 ± 0.50	1.98 ± 0.08	0.89 ± 0.14	200 ± 19	93 ± 16	0.0028
(3) One side 3 g/L PAA	5.21 ± 0.04	1.56 ± 0.18	0.67 ± 0.08	188 ± 12	67 ± 8	0.0023
(4) Both sides 3 g/L PAA	5.33 ± 0.16	1.92 ± 0.17	0.53 ± 0.01	72 ± 12	19 ± 4	0.0020
(5) One side 5 g/L PAA	5.36 ± 0.18	1.58 ± 0.02	0.68 ± 0.02	140 ± 15	42 ± 5	0.0023

However, in this study, better hydrodynamic conditions could reduce the EDL effect, since the 20 mL/min might not be the optimum. This approach has been demonstrated in another study where inducing stirring reduced the R_{EDL} by 52.7% and eliminated the $R_{DB L}$ [58]. Also, since the EDL is related to interface ionic mobility, activating or modifying the membrane surface to induce higher ionic conductivity (reduction in charge build-up) between the membrane and solution interface may decrease the EDL. Generally, in RED system where high electrolyte concentrations are used, the EDL and DBL do not pose significant influence, especially, in AEMs [42].

The time evolution effect of 25 ppm HA on the change in electromembrane resistance was monitored. Generally, the change in resistance increased with time (**Figure 21**). However, this effect was larger in the unmodified membrane than the PAA-AEMs. Thus from zero (0) to 12 minutes, the change in the electrical resistance of the unmodified membrane increased rapidly from 0 Ωcm^2 to 8 Ωcm^2, whereas the 3 g/L modified membrane reached 2.75 Ωcm^2, representing 65.8% improvement. This observation may be attributed to the PAA active negative monolayer repelling the HA, thereby slowing down the adsorption of HA onto the modified membranes, within this short period of studies. This electrostatic repulsion was absent in the unmodified, hence experiencing higher change in the resistance. The results imply that PAA is an effective for reducing HA fouling in modified AEMs that can be applied in RED stacks. However, long term studies on the time evolution of the resistance are required.

It is also interesting to note that the rapid fouling of the unmodified membrane by the negatively charged HA within this short period may be of interest regarding monovalent permselectivity. Thus, the membrane fouled with HA could attain higher sulfate rejection in longer period, since the negative layer of the HA on the membrane may hamper sulfate transport across the membrane. This phenomenon was observed in the mass transport studies conducted in the presence of 25 ppm HA (see **Figure 23**). Thus, we can take advantage of the HA quickly fouling the membranes, especially, the unmodified, to explore the HA electrostatic repulsive impact on other foulants as well as sulfates [114]. It also suggests that deposition of HA on the AEMs would be easier to perform.

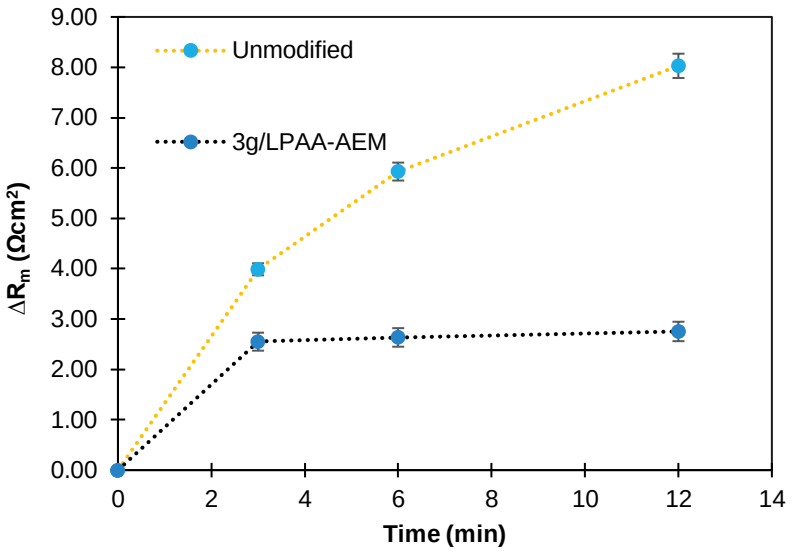

Figure 21 *Change in membrane resistance in the presence of 25 ppm HA*

4.6. MASS TRANSPORT EXPERIMENTS: SULFATE REJECTION STUDY

Sulfate rejection experiments were carried out to evaluate the capability of the different PAA monolayers on sulfate transport restrictions. An improvement in sulfate rejection favor efficient RED process performance. In the absence of HA, the time evolution of sulfate concentration in the feed, *F*, and receiver, *R* compartments is represented in **Figure 22**. Since sulfate is only present in the feed compartment (LCC), the sulfate evolution in the receiver compartment (HCC) was monitored and evaluated for 24 h to follow the sulfate transport through the membranes. The sulfate rejection improved at higher PAA concentrations, though the rejection maximized at 3 g/L PAA both sides modified membrane.

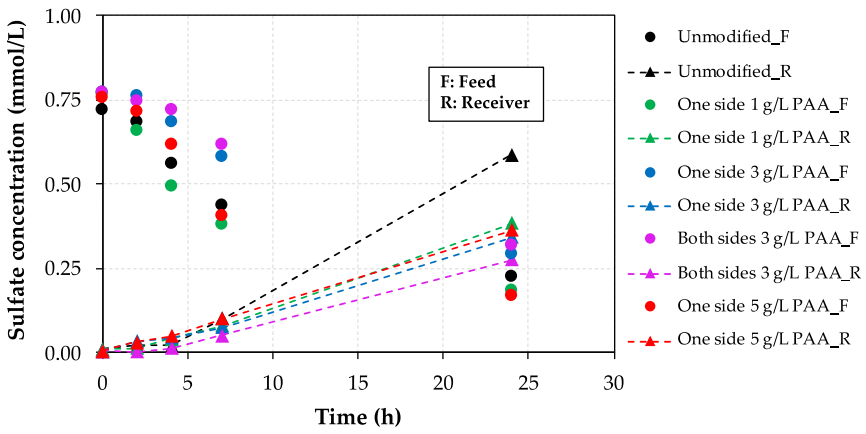

Figure 22 *Sulfate evolution in the absence of HA in feed*

Thus, the rejection of sulfate was 36%, 42%, 39% and 54% enhanced for the one side 1 g/L, 3 g/L, 5 g/L and both sides 3 g/L PAA-AEMs. The sulfate flux at 7 h to 24 h in the unmodified membrane was 197 mmol/(m^2·h), about a half of the flux in the 3 g/L PAA, 104.6 mmol/(m^2·h). The results clearly indicate the ability of the PAA monolayer to improve the membrane monovalent permselectivity for RED applications.

The mass transport experiment was repeated in the presence of 25 ppm HA, as the results are presented. Generally, PAA modified AEMs recorded minimum sulfate concentrations in the receiver compartment at 2 h and 4 h (**Figure 23**), compared to the unmodified. The one side 3 g/L PAA attained a steady lowest sulfate concentration of 0.02 mmol/L in the receiver compartment at 2 h and 4 h. This imply that the it was most effective for sulfate rejection within the first 4 h of 25 ppm HA introduction in the feed. However, at 7 h and 24 h, all the PAA-AEMs lost their effectiveness for sulfate rejection relative to the unmodified. The attachment of large amount of HA on the unmodified layer, might contribute to the better sulfate rejection observed. That is, the attached HA in the absence of PAA interactions might have also formed a negative layer on the unmodified membrane to repel sulphate. However, the unexpected behavior in the PAA-AEMs may be due to the long period interaction of the HA with the PAA monolayer which might have caused loss of the electrostatic attraction between the membrane and the PAA monolayer, leading to lower stability of the PAA. Thus, since the HA also has carboxylic functional groups, its presence might have altered the pH of the solution, protonated the already deprotonated PAA negative monolayer while simultaneously fouling the membrane. In this case, the PAA would be still attached to the AEM if the electrostatic point of attraction if not interrupted but its negative layer would be transformed to COOH, leading to almost neutral charge effect on the membrane surface. If this neutrality occurs, then the entire modified membrane would be incapable of effectively rejecting sulphate, as the SO_4^{2-} permeates the membrane. Another reason may be related to affinity. Thus, this affinity between the AEM fabric or functional groups and the HA might be stronger than the PAA, leading to disruption of the electrostatic attraction between the PAA monolayer and the membrane surface, as the HA advances towards the membrane. Moreover, spectrophotometric analysis was conducted at 280 nm wavelength to measure the HA absorbance to determine its concentration in the receiver with time. The results showed that HA was not present in the receiver compartment, denoting that it was rather attached to the surface of the membrane. This phenomenon was confirmed by observing a dark brownish color on the membrane surface where the 25 ppm of HA was introduced in the mass transport experiment.

The pH might also play a major role in these adverse effects observed in **Figure 23**. In fact, studies on HA adsorption on hydrophobic and hydrophilic membranes reported that HA deposition, adsorption and fouling on membranes is electrostatically favorable in acidic conditions and higher ionic concentrations, while in alkaline conditions, these parameters are rather facilitated by calcium interactions [129, 130]. Another work investigating the effect of pH on HA rejection in NF demonstrated that the grafted PAA strongly rejected the HA at pH 7 whereas weak rejection was reached at pH 3 [131]. Irreversible HA fouling factor was reduced substantially. The better performance of the PAA at higher pH was attributed to the fact that the pKa of HA is 4.75, hence, dissociated at neutral to form a negative layer, strongly

repelling the HA. However, at pH 3, it was less dissociated, therefore, the electrostatic repulsion reduced appreciably. Their results indicate that pH is a very important factor to be considered when dealing with PAA and HA interactions.

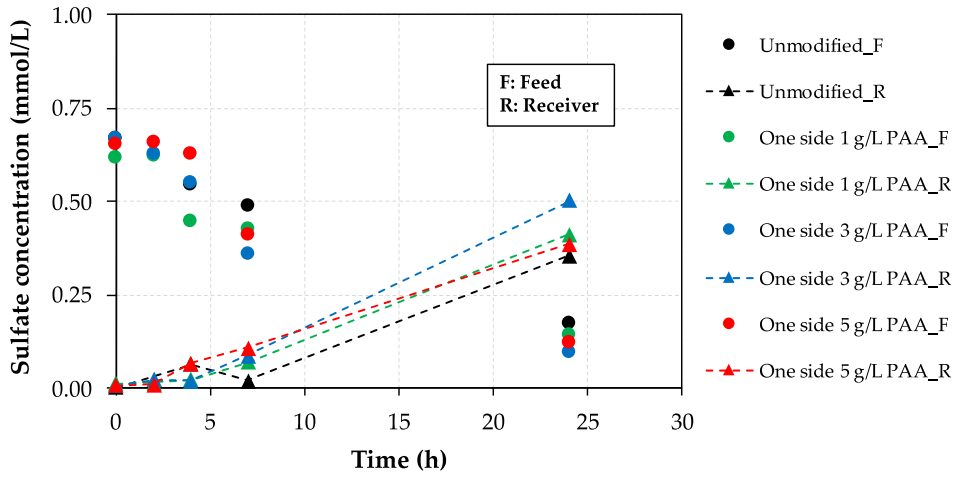

Figure 23 *Sulfate evolution in the presence of HA in feed*

To reduce further disruption of the PAA monolayer by HA, other studies on nanofiltration, ultrafiltration, microfiltration and absorbents modified the membranes using UV irradiation polymerization at short periods, and other methods to generate covalently bonded PAA-membrane interactions instead of electrostatics [130-133], while controlling the pH when the modified membrane was used. In the MF study, a 50 % reduction in natural organic fouling was achieved when HA was used as the model foulant [130]. Regarding the NF analyses, lower HA irreversible fouling factor was attained, and sulfate rejection was improved by 14% [132]. Researchers who used PAA in nanoscale zero-valent iron (NZVI) to reduce the oxidative effect of HA mentioned that the PAA protected the NZVI from HA oxidative attack by 71 % [133]. Thus, our study, together with the literature, denote that the behavior of the PAA-AEMs is clearly badly affected by the presence of organic foulants, which would reduce the efficiency of the RED process performance. However, this can be reduced by inducing covalent bonding between the modifying the PAA and the AEM surface and controlling the pH during operations.

Our results in **Figure 23** suggest that since HA easily fouled the unmodified membrane and resulted in recorded the highest sulfate rejection at 24 h, HA can deliberately be deposited on the AEM to study sulfate rejection effects and antifouling potentials. This novel concept is known as fouling deposition. For instance, researchers deliberately fouled Neosepta AMX with sulfonated poly(2,6-di-methyl-1,4-phenylene oxide) (SPPO) in electrodialysis system. The fouled membrane attained Cl^-/SO_4^{2-} permselectivity coefficient as high as 52.44 [114].

In these contexts of our studies, the application and study of real natural streams of different salinity, which contains different multivalent ions (*i.e.,* Ca^{2+} and Mg^{2+}) as well as different foulants, is essential for further understanding the membrane behavior to develop and implement the RED technology at

industrial scale. The future outlook of this research will cover the design, set-up and long-term operation of a RED stack in order to evaluate the obtainable net power density by using the proposed modified AEMs under real conditions, i.e. using natural feedwaters, which is essential to move forward towards the large-scale implementation of the RED technology

4.7 CLEANING EFFECT ON MEMBRANE ELECTRO -RESISTANCE

The cleaning effect on the ohmic resistance of the membrane and blank (R_{m+s}) was evaluated through EIS analyses, which were performed using 0.5 M NaCl aqueous solutions as the feed and the receiver, and 500 ppm HA as the model foulant. Higher HA concentration was used to really investigate the effect of the fouling and cleaning within the shortest time. As shown in **Figure 24**, both the unmodified and the PAA-AEMs were slightly fouled in the first cycle, even though the HA fouled the unmodified membrane more than the modified. The first cleaning reverted the fouling since the ohmic resistance returned to almost normal values, 17.82 Ωcm^2 and 21.23 Ωcm^2 for the unmodified and modified, respectively. This result might be associated with the fact that HA was not strongly adsorbed onto the membrane surface, hence larger quantity was easily removed by the NaOH. Nevertheless, continues fouling in the second and third cycles increased the R_{m+s} of the modified and unmodified up to 31.3%, and 17.9% sequentially. In this case, the cleaning step reduced the resistance of the fouled unmodified membrane (Unmodified-fouled) by only 2%, and 5% in the PAA-AEMs.

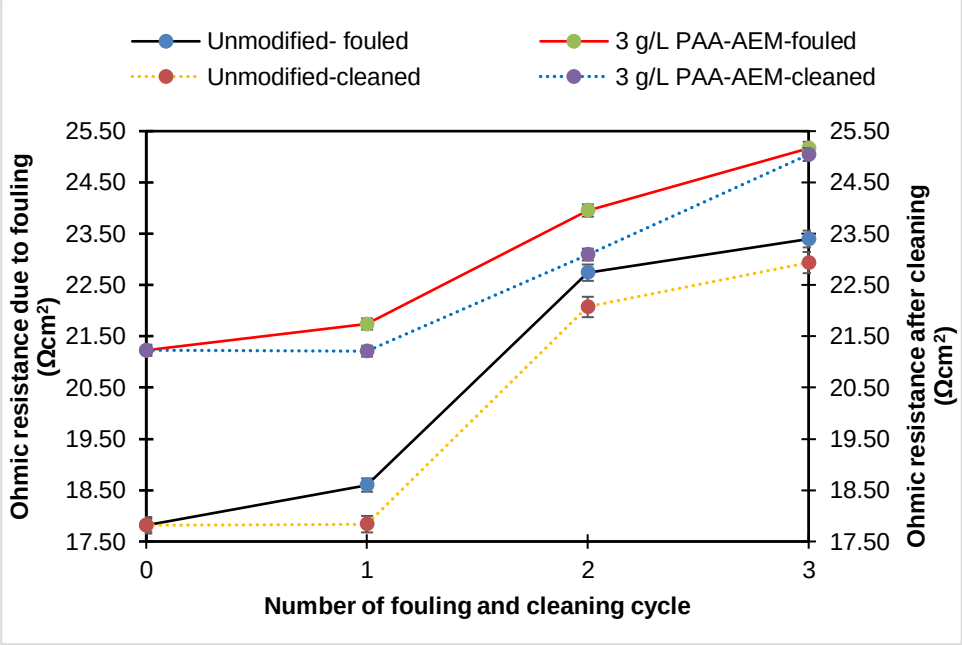

Figure 24 *Effect of repetitive fouling and cleaning on the ohmic resistance*

Thus, the NaOH cleaning could not restore the resistance of the fouled membranes to their original values. This effect can be associated with stronger adsorption of the HA onto the membrane surface as progressive fouling occurs, leading to irreversible fouling. In this respect, the inability of NaOH to clean some organic foulant in AEM has been reported elsewhere [21]. The researchers employed HCl,

and NaOH for the cleaning, and observed that HCl cleaning was more effective than the NaOH with respect to the AEM. Perhaps, an increase in the cleaning time under longer periods is needed to notice appreciable foulant removal. Also, the concentration of the NaOH could be varied to study its effects, though higher concentrations could lead to accelerated aging [134]. Other fouling mitigation approaches employ acid-base, base-acid, and salt solution cleaning, air sparging, and their combinations for reverse electrodialysis and electrodialysis application [87, 89, 90, 120]. These cleaning methods have been mentioned to be effective depending on the nature of the AEM, and the interaction between the AEM and the foulant.

5. CONCLUSIONS AND FUTURE PERSPECTIVES

CONCLUSIONS:

In this study, we explored the surface modification and comprehensive characterization of heterogeneous Ralex AM-PES (Mega a.s.) anion exchange membranes (AEMs), which were modified with a biocompatible poly(acrylic) acid (PAA) as the modifying agent, in different concentrations of 1 g/L to 5 g/L. The modification approach is focused on simultaneously enhancing the antifouling resistance of the AEMs, and the monovalent-anion-permselectivity to achieve an improved Reverse Electrodialysis process performance.

The ATR-FTIR results indicated that the negatively charged PAA monolayer did not react chemically with the polyester-based AEMs, since the polyester functional groups were still present after modification, demonstrating that the attachment was electrostatic. The optimum concentration of PAA was 3 g/L, which exhibited higher hydrophilicity of 34%, and 42% rejection of SO_4^{2-} in the absence of HA. Nevertheless, the presence of HA suppressed the sulfate repulsion capability of all the modified membranes leading to lower sulfate rejection after 24 h. This effect could be attributed to unfavorable change in pH caused by the HA, since PAA electrostatic repulsion against HA decreases in lower pH conditions, hence controlling the pH is important.

The swelling degree related to the membrane thickness and the diameter, increased by 36-38 %, and 5 % consecutively, in all the membranes, indicating the need to control membrane swelling since it contributes to higher electro-membrane resistance, which affects the RED process efficiency. Regarding the cyclic voltammetry results, the modified membranes exhibited higher current-voltage profiles due to their improved hydrophilicity. This corresponded to a higher overall transport of anions across the modified membranes.

The two methods employed for the ion exchange capacity (IEC) measurements suggest that the Mohr's titration method have lower IEC values and less accuracy than spectrophotometric technique, which denotes that the IEC of the membranes strongly depends on the method considered. The results suggest that spectrophotometric method can be more reliable for determining IEC of modified AEMs.

The membrane electro-resistances, double-layer resistances and diffusion boundary layer resistances of the different modified membranes were in the same order of magnitude: 5.0-5.4 $\Omega \cdot cm^2$, 1.6-1.9 $\Omega \cdot cm^2$, and 0.5-0.9 $\Omega \cdot cm^2$, respectively, compared to the values for the unmodified AEM, indicating that the modification did not appreciably increase the membrane resistance. Therefore, the PAA negative

monolayer uncompromised the electrical conductivity of the different prepared modified membranes. The order of magnitude of the electro-resistances of the modified membrane are comparable to those reported in literature for both modified heterogeneous and homogeneous anion exchange membranes. The results of the fouling evolution of the membranes showed that the membranes were susceptible to HA fouling, even when a low concentration (25 ppm) of the model foulant was considered. However, within 12 minutes, the change in the electrical resistance of the unmodified membrane elevated swiftly from 0 Ωcm^2 to 8 Ωcm^2, whereas the one side 3 g/L modified membrane reached 2.75 $\Omega cm^{2,}$ representing 65.8% antifouling potential. This suggests that the antifouling potential of the PAA modified membrane was improved in comparison with the pristine membrane.

Since cleaning is also essential for fouling mitigation, repetitive fouling and cleaning of the membranes were investigated, using 0.1 M NaOH aqueous solutions as the cleaning agent. The NaOH reverted the membrane resistance to the original value after the first fouling and cleaning step. However, only 2-5% restoration was achieved in the subsequent fouling and cleaning steps, leading to higher membrane resistance. The results imply that irreversible fouling occurred during the second and third cleaning steps.

FUTURE PERSPECTIVES:

Although this study provides novel insights and basic knowledge for the progressive development of hydrophilic, eco-friendly, stable and durable functionalized AEMs for an improved reverse electrodialysis performance, the following challenges need to be considered to make this electro-membrane process preferable for industrial application in the future:

- Understanding the fouling mechanisms and collective behavior of foulants under natural saline streams conditions, to allow for comprehensive fouling monitoring, and mitigation.
- Development of appropriate pre-treatment, post treatment and cleaning strategies to increase membrane stability, durability and re-usability.
- Comprehensive postmortem analysis such as change in zeta potential, elemental analysis, SEM, and AFM of the fouled membranes to properly understand the nature and interaction between the foulant the membrane.
- Design of ecofriendly, less expensive tailor-made, and readily tunable AEMs for optimum modification results.
- Graft polymerization to induce covalent bonding between the PAA and the AEMs instead of the relatively weaker electrostatic attraction which are highly influenced by the ionic strength and pH of the solution. This will reduce the loss of PAA monolayer from the membrane surface.
- Introduction of the PAA negative layer on the AEM via double layer or layer-by-layer modification to enhance the repulsive strength of the modified membrane.
- Activation of the membrane surface to facilitate faster ionic transport.
- Taking advantage of the adverse effect of membrane fouling by HA (hydrophobic) or other hydrophilic foulants to explore fouling deposition technique which could improve the monovalent permselectivity of the membrane and the antifouling potential through electrostatic repulsion.

6. REFERENCES

1. Pandey, P. and R.S. Chauhan, *Membranes for gas separation.* Progress in Polymer Science, 2001. **26**(6): p. 853-893.
2. Loeb, S. and S. Sourirajan, *Sea Water Demineralization by Means of an Osmotic Membrane*, in *Saline Water Conversion—II*. 1963, AMERICAN CHEMICAL SOCIETY. p. 117-132.
3. Souriyajan, S., Matsuura, T. , *Reverse Osmosis/Ultrafiltration process and principle*, N.R.C.o. Canada, Editor. 1985: Canada.
4. IPCC, C.C., *The Physical Science Basis, Summary for Policymakers*. 2007.
5. Laboratory, G.M., *Trends in Atmospheric Carbon Dioxide*. 2020.
6. Farrell, E., et al., *Reverse electrodialysis powered greenhouse concept for water- and energy-self-sufficient agriculture.* Applied Energy, 2017. **187**: p. 390-409.
7. Rafiee, A. and K.R. Khalilpour, *Chapter 11 - Renewable Hybridization of Oil and Gas Supply Chains*, in *Polygeneration with Polystorage for Chemical and Energy Hubs*, K.R. Khalilpour, Editor. 2019, Academic Press. p. 331-372.
8. IEA, *Global Energy Review* 2020.
9. Ramon, G.Z., B.J. Feinberg, and E.M.V. Hoek, *Membrane-based production of salinity-gradient power.* Energy & Environmental Science, 2011. **4**(11): p. 4423-4434.
10. Garland, N.L., D.C. Papageorgopoulos, and J.M. Stanford, *Hydrogen and Fuel Cell Technology: Progress, Challenges, and Future Directions.* Energy Procedia, 2012. **28**: p. 2-11.
11. Yip, N.Y., et al., *Salinity Gradients for Sustainable Energy: Primer, Progress, and Prospects.* Environ Sci Technol, 2016. **50**(22): p. 12072-12094.
12. Post, J.W., et al., *Salinity-gradient power: Evaluation of pressure-retarded osmosis and reverse electrodialysis.* Journal of Membrane Science, 2007. **288**(1): p. 218-230.
13. Wick G.L., S.W.R., *Prospects for renewable energy from the sea.* Marine Technology Society Journal, 1977. **11**: p. 16-21.
14. Güler, E., et al., *Performance-determining membrane properties in reverse electrodialysis.* Journal of Membrane Science, 2013. **446**: p. 266-276.
15. Dlugolecki, P., et al., *Current status of ion exchange membranes for power generation from salinity gradients.* Journal of Membrane Science, 2008. **319**(1-2): p. 214-222.
16. A.R. Khodabakhshi, S.S.M., S.M. Hosseini *Preparation and characterization of monovalent ion-selective poly (vinyl chloride)-blend-poly (styrene-co-butadiene) heterogeneous anion-exchange membranes* Polym. Int., 2011. **60**: p. 466-474.
17. Lee, H.-J., et al., *Fouling of an anion exchange membrane in the electrodialysis desalination process in the presence of organic foulants.* Desalination, 2009. **238**(1): p. 60-69.
18. de Bonis, C., et al., *Enhancement of proton mobility and mitigation of methanol crossover in sPEEK fuel cells by an organically modified titania nanofiller.* Journal of Solid State Electrochemistry, 2016. **20**(6): p. 1585-1598.
19. Bazinet, L., et al., *Identification of Skim Milk Electroacidification Fouling: A Microscopic Approach.* Journal of Colloid and Interface Science, 2001. **237**(1): p. 62-69.
20. Korngold, E., et al., *Fouling of anionselective membranes in electrodialysis.* Desalination, 1970. **8**(2): p. 195-220.
21. Guo, H., et al., *Mechanisms of chemical cleaning of ion exchange membranes: A case study of plant-scale electrodialysis for oily wastewater treatment.* Journal of Membrane Science, 2015. **496**: p. 310-317.
22. Post, J.W., H.V.M. Hamelers, and C.J.N. Buisman, *Influence of multivalent ions on power production from mixing salt and fresh water with a reverse electrodialysis system.* Journal of Membrane Science, 2009. **330**(1): p. 65-72.
23. Vermaas, D.A., et al., *Fouling in reverse electrodialysis under natural conditions.* (1879-2448 (Electronic)).
24. Pintossi, D., et al., *Influence of sulfate on anion exchange membranes in reverse electrodialysis.* npj Clean Water, 2020. **3**(1).

25. Wenten, I.G., Khoiruddin, K. , *Recent developments in heterogeneous ion-exchange membrane: preparation, modification, characterization and performance evaluation.* J Eng Sci Technol, 2016. **11**: p. 916-934.
26. Güler, E., et al., *Monovalent-ion-selective membranes for reverse electrodialysis.* Journal of Membrane Science, 2014. **455**: p. 254-270.
27. Vaselbehagh, M., et al., *Improved antifouling of anion-exchange membrane by polydopamine coating in electrodialysis process.* Desalination, 2014. **332**(1): p. 126-133.
28. Kotoka, F., Merino-Garcia, I., and Velizarov, S., *Surface Modifications of Anion Exchange Membranes for an Improved Reverse Electrodialysis Process Performance: A Review.* Membranes, 2020. **10**(8).
29. Merino-Garcia, I., et al., *Characterization of Poly(Acrylic) Acid-Modified Heterogenous Anion Exchange Membranes with Improved Monovalent Permselectivity for RED.* Membranes (Basel), 2020. **10**(6).
30. Vaselbehagh, M., et al., *Surface modification of an anion exchange membrane to improve the selectivity for monovalent anions in electrodialysis – experimental verification of theoretical predictions.* Journal of Membrane Science, 2015. **490**: p. 301-310.
31. Zhao, Y., et al., *Mimicking the cell membrane: bio-inspired simultaneous functions with monovalent anion selectivity and antifouling properties of anion exchange membrane.* Scientific Reports, 2016. **6**(1): p. 37285.
32. Lee, J.-S., et al., *Surface modification of Nafion membranes by ion implantation to reduce methanol crossover in direct methanol fuel cells.* RSC Advances, 2016. **6**(67): p. 62467-62470.
33. Mikhaylin, S. and L. Bazinet, *Fouling on ion-exchange membranes: Classification, characterization and strategies of prevention and control.* Adv Colloid Interface Sci, 2016. **229**: p. 34-56.
34. Daraei, P., et al., *Fabrication of PES nanofiltration membrane by simultaneous use of multi-walled carbon nanotube and surface graft polymerization method: Comparison of MWCNT and PAA modified MWCNT.* Separation and Purification Technology, 2013. **104**: p. 32-44.
35. Gümüşoğlu, T., G.A. Arı, and H. Deligöz, *Investigation of salt addition and acid treatment effects on the transport properties of ionically cross-linked polyelectrolyte complex membranes based on chitosan and polyacrylic acid.* Journal of Membrane Science, 2011. **376**(1-2): p. 25-34.
36. Madaeni, S.S., S. Zinadini, and V. Vatanpour, *A new approach to improve antifouling property of PVDF membrane using in situ polymerization of PAA functionalized TiO2 nanoparticles.* Journal of Membrane Science, 2011. **380**(1-2): p. 155-162.
37. Moghadassi, A.R., et al., *Surface modification of heterogeneous cation exchange membrane through simultaneous using polymerization of PAA and multi walled carbon nano tubes.* Journal of Industrial and Engineering Chemistry, 2014. **20**(5): p. 2710-2718.
38. Zhao, Y., et al., *An anion exchange membrane modified by alternate electro-deposition layers with enhanced monovalent selectivity.* Journal of Membrane Science, 2016. **520**: p. 262-271.
39. Kedem, O., et al., *Low-polarisation electrodialysis membranes.* Desalination, 1998. **118**(1): p. 305-314.
40. Veerman, J., et al., *Reverse electrodialysis: Performance of a stack with 50 cells on the mixing of sea and river water.* Journal of Membrane Science, 2009. **327**(1): p. 136-144.
41. Wick, G.L., *Power from salinity gradients.* Energy, 1978. **3**(1): p. 95-100.
42. Długołęcki, P., et al., *On the resistances of membrane, diffusion boundary layer and double layer in ion exchange membrane transport.* Journal of Membrane Science, 2010. **349**(1-2): p. 369-379.
43. Tedesco, M., et al., *Performance of the first reverse electrodialysis pilot plant for power production from saline waters and concentrated brines.* Journal of Membrane Science, 2016. **500**: p. 33-45.

44. Besha, A.T., et al., *Design of Monovalent Ion Selective Membranes for Reducing the Impacts of Multivalent Ions in Reverse Electrodialysis.* Membranes (Basel), 2019. **10**(1).
45. Saracco, G., *Transport properties of monovalent-ion-permselective membranes.* Chemical Engineering Science, 1997. **52**(17): p. 3019-3031.
46. Tian, H., et al., *Unique applications and improvements of reverse electrodialysis: A review and outlook.* Applied Energy, 2020. **262**.
47. Lee, H.-J., et al., *Effects of silica sol on ion exchange membranes: Electrochemical characterization of anion exchange membranes in electrodialysis of silica sol containing-solutions.* Korean Journal of Chemical Engineering, 2003. **20**(5): p. 889-895.
48. Brunelle, M.T., *Colloidal fouling of reverse osmosis membranes.* Desalination, 1980. **32**: p. 127-135.
49. Bleha, M., et al., *Characteristic of the critical state of membranes in ED-desalination of milk whey.* Desalination, 1992. **86**(2): p. 173-186.
50. Banasiak, L.J. and A.I. Schäfer, *Removal of boron, fluoride and nitrate by electrodialysis in the presence of organic matter.* Journal of Membrane Science, 2009. **334**(1): p. 101-109.
51. R., A., *Fouling of ion-selective membranes during electrodialysis of grape must.* J Membr Sci 1989. **41**: p. 115-126.
52. T., T., *Encyclopedia of Colloid and Interface Science*. 1 ed. 2013: Springer-Verlag Berlin Heidelberg. XI, 1436.
53. Zhang, W., et al., *Investigations on electrochemical properties of membrane systems in ion-exchange membrane transport processes by electrochemical impedance spectroscopy and direct current measurements.* Electrochimica Acta, 2016. **216**: p. 110-119.
54. Macdonald, D.D., *Reflections on the history of electrochemical impedance spectroscopy.* Electrochimica Acta, 2006. **51**(8-9): p. 1376-1388.
55. Zhang, W., et al., *Investigations on the interfacial capacitance and the diffusion boundary layer thickness of ion exchange membrane using electrochemical impedance spectroscopy.* Journal of Membrane Science, 2016. **502**: p. 37-47.
56. Córdoba-Torres, P., T.J. Mesquita, and R.P. Nogueira, *Influence of geometry-induced current and potential distributions on the characterization of constant-phase element behavior.* Electrochimica Acta, 2013. **87**: p. 676-685.
57. Córdoba-Torres, P., et al., *On the intrinsic coupling between constant-phase element parameters α and Q in electrochemical impedance spectroscopy.* Electrochimica Acta, 2012. **72**: p. 172-178.
58. Park, J.S., et al., *An electrical impedance spectroscopic (EIS) study on transport characteristics of ion-exchange membrane systems.* J Colloid Interface Sci, 2006. **300**(2): p. 655-62.
59. Jonscher, A.K., *Dielectric relaxation in solids.* Journal of Physics D: Applied Physics, 1999. **32**(14): p. R57-R70.
60. Sweity, A., et al., *Relation between EPS adherence, viscoelastic properties, and MBR operation: Biofouling study with QCM-D.* Water Res, 2011. **45**(19): p. 6430-40.
61. Ivnitsky, H., et al., *Bacterial community composition and structure of biofilms developing on nanofiltration membranes applied to wastewater treatment.* Water Res, 2007. **41**(17): p. 3924-35.
62. Ruiz, B., et al., *Application of relaxation periods during electrodialysis of a casein solution: Impact on anion-exchange membrane fouling.* Journal of Membrane Science, 2007. **287**(1): p. 41-50.
63. Liu, C.X., et al., *Modification of membrane surface for anti-biofouling performance: Effect of anti-adhesion and anti-bacteria approaches.* Journal of Membrane Science, 2010. **346**(1): p. 121-130.
64. Sosa-Fernandez, P.A., et al., *Influence of solution composition on fouling of anion exchange membranes desalinating polymer-flooding produced water.* J Colloid Interface Sci, 2019. **557**: p. 381-394.

65. Lteif, R., et al., *Conductivitéélectrique membranaire: étude de l'effet de la concentration, de la nature de l'électrolyte et de la structure membranaire.* European Polymer Journal, 1999. **35**(7): p. 1187-1195.
66. Belaid, N.N., et al., *Conductivité membranaire: interprétation et exploitation selon le modèle à solution interstitielle hétérogène.* European Polymer Journal, 1999. **35**(5): p. 879-897.
67. Mulyati, S., et al., *Simultaneous improvement of the monovalent anion selectivity and antifouling properties of an anion exchange membrane in an electrodialysis process, using polyelectrolyte multilayer deposition.* Journal of Membrane Science, 2013. **431**: p. 113-120.
68. Gao, H., et al., *Monovalent-anion selective and antifouling polyelectrolytes multilayer anion exchange membrane for reverse electrodialysis.* Journal of Membrane Science, 2018. **567**: p. 68-75.
69. Park, J.S., et al., *An approach to fouling characterization of an ion-exchange membrane using current-voltage relation and electrical impedance spectroscopy.* J Colloid Interface Sci, 2006. **294**(1): p. 129-38.
70. Pintossi, D., et al., *Electrochemical impedance spectroscopy of a reverse electrodialysis stack: A new approach to monitoring fouling and cleaning.* Journal of Power Sources, 2019. **444**.
71. Pismenskaia, N., et al., *Chronopotentiometry applied to the study of ion transfer through anion exchange membranes.* Journal of Membrane Science, 2004. **228**(1): p. 65-76.
72. Lee, H., et al., *Analysis of fouling potential in the electrodialysis process in the presence of an anionic surfactant foulant.* Journal of Membrane Science, 2008. **325**(2): p. 719-726.
73. Mishchuk, N.A., *Concentration polarization of interface and non-linear electrokinetic phenomena.* Advances in colloid and interface science, 2010. **160**(1-2): p. 16-39.
74. Choi, J.-H., S.-H. Kim, and S.-H. Moon, *Heterogeneity of Ion-Exchange Membranes: The Effects of Membrane Heterogeneity on Transport Properties.* Journal of Colloid and Interface Science, 2001. **241**(1): p. 120-126.
75. Tanaka, N., M. Nagase, and M. Higa, *Organic fouling behavior of commercially available hydrocarbon-based anion-exchange membranes by various organic-fouling substances.* Desalination, 2012. **296**: p. 81-86.
76. Cao, R., et al., *The properties and antifouling performance of anion exchange membranes modified by polydopamine and poly (sodium 4-styrenesulfonate).* Colloids and Surfaces A: Physicochemical and Engineering Aspects, 2020. **589**.
77. Mulyati, S., et al., *Improvement of the antifouling potential of an anion exchange membrane by surface modification with a polyelectrolyte for an electrodialysis process.* Journal of Membrane Science, 2012. **417-418**: p. 137-143.
78. Wang, X.-l., et al., *Surface Modification of Anion Exchange Membrane by Covalent Grafting for Imparting Permselectivity between Specific Anions.* Electrochimica Acta, 2015. **174**: p. 1113-1121.
79. Kusumoto, K., Y. Mizumoto, and Y. Mizutani, *Modification of anion exchange membranes by oxidation of selected chemical sites for the purpose of preventing fouling during dialysis.* Desalination, 1975. **17**(3): p. 303-311.
80. Zembala, M., *Electrokinetics of heterogeneous interfaces.* Advances in Colloid and Interface Science, 2004. **112**(1): p. 59-92.
81. Delgado, A.V., et al., *Measurement and interpretation of electrokinetic phenomena.* Journal of Colloid and Interface Science, 2007. **309**(2): p. 194-224.
82. Lee, W., et al., *Evaluation of surface properties of reverse osmosis membranes on the initial biofouling stages under no filtration condition.* Journal of Membrane Science, 2010. **351**(1): p. 112-122.
83. Park, J.-S., H.-J. Lee, and S.-H. Moon, *Determination of an optimum frequency of square wave power for fouling mitigation in desalting electrodialysis in the presence of humate.* Separation and Purification Technology, 2003. **30**(2): p. 101-112.

84. Kim, D.H., S.-H. Moon, and J. Cho, *Investigation of the adsorption and transport of natural organic matter (NOM) in ion-exchange membranes.* Desalination, 2003. **151**(1): p. 11-20.
85. Lee, H.-J., et al., *Characterization of anion exchange membranes fouled with humate during electrodialysis.* Journal of Membrane Science, 2002. **203**(1): p. 115-126.
86. Park, J.-S., et al., *Fouling mitigation of anion exchange membrane by zeta potential control.* Journal of Colloid and Interface Science, 2003. **259**(2): p. 293-300.
87. Langevin, M.-E. and L. Bazinet, *Ion-exchange membrane fouling by peptides: A phenomenon governed by electrostatic interactions.* Journal of Membrane Science, 2011. **369**(1-2): p. 359-366.
88. Guo, H., et al., *Analysis of anion exchange membrane fouling mechanism caused by anion polyacrylamide in electrodialysis.* Desalination, 2014. **346**: p. 46-53.
89. Vermaas, D.A., et al., *Periodic feedwater reversal and air sparging as antifouling strategies in reverse electrodialysis.* Environ Sci Technol, 2014. **48**(5): p. 3065-73.
90. Xia, Q., et al., *Study on the fouling mechanism and cleaning method in the treatment of polymer flooding produced water with ion exchange membranes.* RSC Advances, 2018. **8**(52): p. 29947-29957.
91. Ruan, H., et al., *Mussel-inspired sulfonated polydopamine coating on anion exchange membrane for improving permselectivity and anti-fouling property.* Journal of Membrane Science, 2018. **550**: p. 427-435.
92. Zhao, Y., et al., *A chemically assembled anion exchange membrane surface for monovalent anion selectivity and fouling reduction.* Journal of Materials Chemistry A, 2019. **7**(11): p. 6348-6356.
93. Deng, J., et al., *Developments and new applications of UV-induced surface graft polymerizations.* Progress in Polymer Science, 2009. **34**(2): p. 156-193.
94. Ahmad, M., et al., *Layer-by-layer modification of aliphatic polyamide anion-exchange membranes to increase Cl−/SO42− selectivity.* Journal of Membrane Science, 2019. **578**: p. 209-219.
95. Zhao, Y., C. Gao, and B. Van der Bruggen, *Technology-driven layer-by-layer assembly of a membrane for selective separation of monovalent anions and antifouling.* Nanoscale, 2019. **11**(5): p. 2264-2274.
96. Zhao, Y., et al., *Electric-pulse layer-by-layer assembled of anion exchange membrane with enhanced monovalent selectivity.* Journal of Membrane Science, 2018. **548**: p. 81-90.
97. Zhang, Y., et al., *Composite anion exchange membrane made by layer-by-layer method for selective ion separation and water migration control.* Separation and Purification Technology, 2018. **192**: p. 278-286.
98. Xu, T., *Ion exchange membranes: State of their development and perspective.* Journal of Membrane Science, 2005. **263**(1-2): p. 1-29.
99. Hagesteijn, K.F.L., S. Jiang, and B.P. Ladewig, *A review of the synthesis and characterization of anion exchange membranes.* Journal of Materials Science, 2018. **53**(16): p. 11131-11150.
100. Luo, T., S. Abdu, and M. Wessling, *Selectivity of ion exchange membranes: A review.* Journal of Membrane Science, 2018. **555**: p. 429-454.
101. Nagarale, R.K., et al., *Development of urethane acrylate composite ion-exchange membranes and their electrochemical characterization.* J Colloid Interface Sci, 2004. **270**(2): p. 446-54.
102. Shahkaramipour, N., et al., *Membranes with Surface-Enhanced Antifouling Properties for Water Purification.* Membranes (Basel), 2017. **7**(1).
103. Pawlowski, S., et al., *On operation of reverse electrodialysis (RED) and membrane capacitive deionisation (MCDI) with natural saline streams: A critical review.* Desalination, 2020. **476**.
104. Khoiruddin, et al., *Surface modification of ion-exchange membranes: Methods, characteristics, and performance.* Journal of Applied Polymer Science, 2017. **134**(48).

105. Sata, T., T. Yamaguchi, and K. Matsusaki, *Interaction between anionic polyelectrolytes and anion exchange membranes and change in membrane properties.* Journal of Membrane Science, 1995. **100**(3): p. 229-238.
106. Grebenyuk, V.D., et al., *Surface modification of anion-exchange electrodialysis membranes to enhance anti-fouling characteristics.* Desalination, 1998. **115**(3): p. 313-329.
107. De Giglio, E., et al., *Biocompatibility of Poly(Acrylic Acid) Thin Coatings Electro-synthesized onto TiAlV-based Implants.* Journal of Bioactive and Compatible Polymers, 2010. **25**(4): p. 374-391.
108. Diken, M.E., et al., *Synthesis and Characterization of Poly(Acrylic Acid)/Organo-Modified Nanohydroxyapatite Nanocomposites: Thermal, Optical and Biocompatibility Properties.* Advances in Materials Science, 2018. **18**(3): p. 54-67.
109. Nebavskaya, X., et al., *Electrochemical Properties of Homogeneous and Heterogeneous Anion Exchange Membranes Coated with Cation Exchange Polyelectrolyte.* Membranes (Basel), 2019. **9**(1).
110. Pan, J., et al., *Preparation of a monovalent selective anion exchange membrane through constructing a covalently crosslinked interface by electro-deposition of polyethyleneimine.* Journal of Membrane Science, 2017. **539**: p. 263-272.
111. Li, Y., et al., *Improvement of the antifouling performance and stability of an anion exchange membrane by surface modification with graphene oxide (GO) and polydopamine (PDA).* Journal of Membrane Science, 2018. **566**: p. 44-53.
112. Li, Y., et al., *Modification and properties characterization of heterogeneous anion-exchange membranes by electrodeposition of graphene oxide (GO).* Applied Surface Science, 2018. **442**: p. 700-710.
113. Zhao, Z., et al., *Characterization of anion exchange membrane modified by electrodeposition of polyelectrolyte containing different functional groups.* Desalination, 2016. **386**: p. 58-66.
114. Jiang, C., et al., *Fouling deposition as an effective approach for preparing monovalent selective membranes.* Journal of Membrane Science, 2019. **580**: p. 327-335.
115. Fernandez-Gonzalez, C., et al., *Enhancing fouling resistance of polyethylene anion exchange membranes using carbon nanotubes and iron oxide nanoparticles.* Desalination, 2017. **411**: p. 19-27.
116. Guler, E., et al., *Tailor-made anion-exchange membranes for salinity gradient power generation using reverse electrodialysis.* ChemSusChem, 2012. **5**(11): p. 2262-70.
117. Karas, F., et al., *Determination of the ion-exchange capacity of anion-selective membranes.* International Journal of Hydrogen Energy, 2014. **39**(10): p. 5054-5062.
118. Østedgaard-Munck, D.N., et al., *Data on flow cell optimization for membrane-based electrokinetic energy conversion.* Data in Brief, 2017. **15**: p. 1-11.
119. Østedgaard-Munck, D.N., et al., *Membrane-based electrokinetic energy conversion.* Materials Today Energy, 2017. **5**: p. 118-125.
120. Bdiri, M., et al., *Cleaning of cation-exchange membranes used in electrodialysis for food industry by chemical solutions.* Separation and Purification Technology, 2018. **199**: p. 114-123.
121. Villafana-Lopez, L., et al., *Custom-Made Ion Exchange Membranes at Laboratory Scale for Reverse Electrodialysis.* Membranes (Basel), 2019. **9**(11).
122. Manatunga, D.C., R.M. de Silva, and K.M.N. de Silva, *Double layer approach to create durable superhydrophobicity on cotton fabric using nano silica and auxiliary non fluorinated materials.* Applied Surface Science, 2016. **360**: p. 777-788.
123. Ahmadi, E., et al., *Enhanced anticancer potency by combination chemotherapy of HT-29 cells with biodegradable, pH-sensitive nanoparticles for co-delivery of hydroxytyrosol and doxorubicin.* Journal of Drug Delivery Science and Technology, 2019. **51**: p. 721-735.
124. Memon, A.A., et al., *Synthesis of highly photo-catalytic and electro-catalytic active textile structured carbon electrode and its application in DSSCs.* Solar Energy, 2017. **150**: p. 521-531.

125. Parvinzadeh, M. and I. Ebrahimi, *Influence of atmospheric-air plasma on the coating of a nonionic lubricating agent on polyester fiber.* Radiation Effects and Defects in Solids, 2011. **166**(6): p. 408-416.
126. Alvarez-Gayosso, C., et al., *Preparation and microstructure of cobalt(III) poly (acrylate) hybrid materials.* International Journal of Basic and Applied Sciences, 2015. **4**(3).
127. Brožová, L., et al., *The influence of activation of heterogeneous ion-exchange membranes on their electrochemical properties.* Desalination and Water Treatment, 2014: p. 1-5.
128. Vaselbehagh, M., et al., *Biofouling phenomena on anion exchange membranes under the reverse electrodialysis process.* Journal of Membrane Science, 2017. **530**: p. 232-239.
129. Yuan, W. and A.L. Zydney, *Effects of solution environment on humic acid fouling during microfiltration.* Desalination, 1999. **122**(1): p. 63-76.
130. Carroll, T., N.A. Booker, and J. Meier-Haack, *Polyelectrolyte-grafted microfiltration membranes to control fouling by natural organic matter in drinking water.* Journal of Membrane Science, 2002. **203**(1): p. 3-13.
131. Abu Seman, M.N., et al., *Reduction of nanofiltration membrane fouling by UV-initiated graft polymerization technique.* Journal of Membrane Science, 2010. **355**(1-2): p. 133-141.
132. Abuhabib, A.A., et al., *Nanofiltration membrane modification by UV grafting for salt rejection and fouling resistance improvement for brackish water desalination.* Desalination, 2012. **295**: p. 16-25.
133. Kim, H.S., et al., *Effect of anions and humic acid on the performance of nanoscale zero-valent iron particles coated with polyacrylic acid.* Chemosphere, 2014. **113**: p. 93-100.
134. Garcia-Vasquez, W., et al., *Effects of acid–base cleaning procedure on structure and properties of anion-exchange membranes used in electrodialysis.* Journal of Membrane Science, 2016. **507**: p. 12-23.
135. Wang, M., et al., *An attempt for improving electrodialytic transport properties of a heterogeneous anion exchange membrane.* Desalination, 2014. **351**: p. 163-170.
136. Zhao, Y., et al., *Sulfonated reduced graphene oxide modification layers to improve monovalent anions selectivity and controllable resistance of anion exchange membrane.* Journal of Membrane Science, 2017. **536**: p. 167-175.

APPENDIX

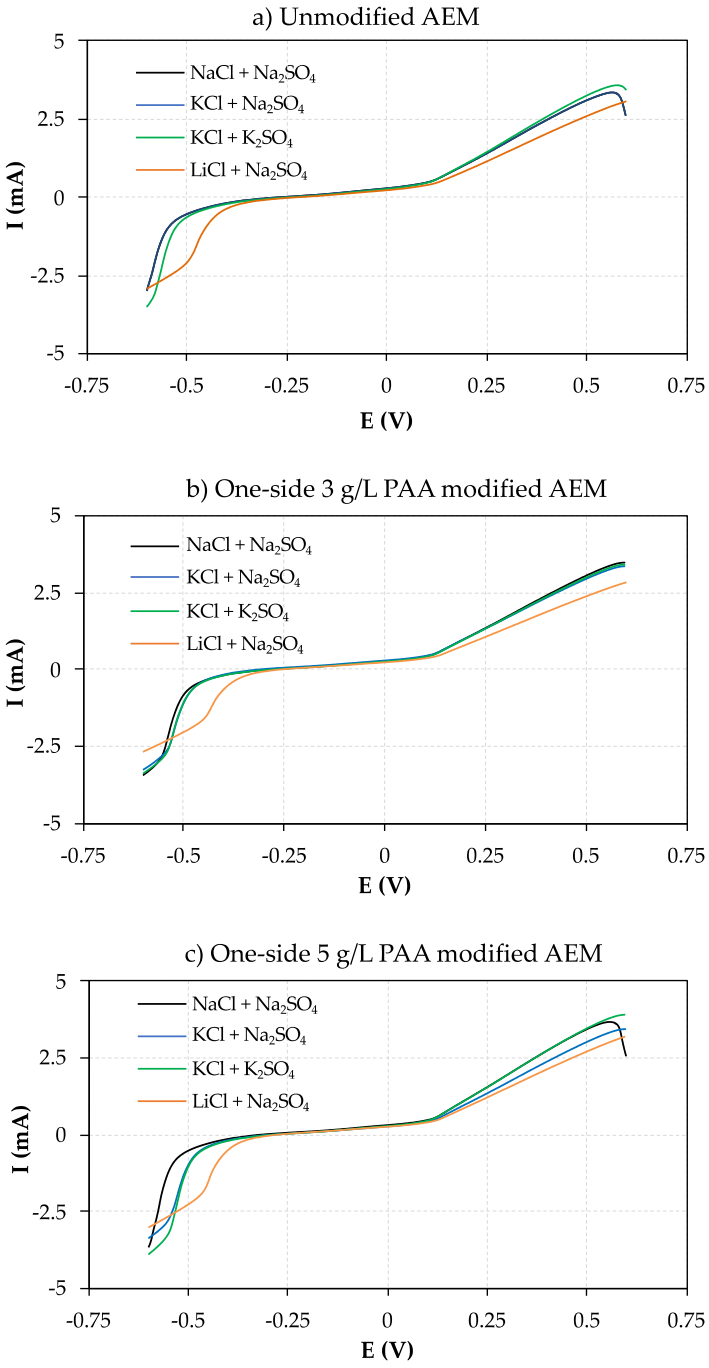

APPENDIX A1 LSV current-voltage profile showing effect of the co-ion present in the feed chamber as a function of the AEM used: a) unmodified; b) one side 3 g/L PAA modified; and c) one side 5 g/L PAA modified

APPENDIX A2 Fit parameters of EIS from Equivalent Circuit Model (Feed 0.017NaCl +0.1g/LNa_2SO_4; Receiver 0.5NaCl)

Sample (Ralex AEM)	$R_m(\Omega cm^2)$	$R_{EDL}(\Omega cm^2)$	$R_{DBL}(\Omega cm^2)$	$C_{EDL}(F)$	$C_{DBL}(F)$	χ^2.
Unmodified	37.67±0.04	12.59±0.21	0.38±0.15	1.17×10^{-3}	9.51×10^{-4}	3.0×10^{-3}
One side 1g/L PAA	38.38±0.03	14.50±0.04	1.33±0.01	8.25×10^{-4}	5.49×10^{-4}	3.6×10^{-3}
One side 3g/L PAA	40.73±0.07	12.94±0.21	1.06±0.00	9.13×10^{-4}	7.24×10^{-4}	2.60×10^{-3}
Two sides 3g/L PAA	30.49±0.05	16.91±0.41	0.75±0.00	1.06×10^{-3}	7.43×10^{-4}	2.2×10^{-3}
One side 5g/L PAA	31.66±0.04	15.04±0.53	0.22±0.00	1.35×10^{-3}	1.05×10^{-3}	1.75×10^{-3}

APPENDIX A3 Total electrical resistance measured by direct current

Sample (Ralex AEM)	$R_m(\Omega cm^2)$
Unmodified	6.89±0.10
One side 1g/L PAA	7.47±0.33
One side 3g/L PAA	8.13±0.37
Two sides 3g/L PAA	8.62±0.49
One side 5g/L PAA	8.42±0.27

Appendix A4 Comparison of the membrane resistance values obtained in this study with those reported in literature for other commercial AEMs before and after modification

AEM type	Modification approach	R_M before modification ($\Omega\cdot cm^2$)	R_M after modification ($\Omega\cdot cm^2$)	Reference
Heterogeneous Ralex AM-PES (Mega a.s.)	Direct contact /immersion	5.01	5.1-5.4	This study
Heterogeneous (Zhe-jiang Qianqui Environmental Protection & Water Treatment Co. Ltd., China)	LbL deposition	4.5	4.8	[135]
Neosepta AMX (Astom Corp.)	Dip coating	1.2	2.9	[30]
Neosepta AMX (Astom Corp.)	Immersion	2.5	5.0	[27, 128]
Homogeneous Neosepta ASE (Astom Corp.)	Immersion (co-deposition)	3.6	4.5	[76]
Homogeneous JAM-II-07 (Yanrun, China)	Coating by deposition	3.1	3.7	[136]
Homogeneous Type 1Fujifilm	Self-adhesion deposition	1.0	6.8	[91]
Ionics	Coating by adsorption	2.5	5.7	[106]